# The bitumen formation and Re-Os characteristics of a $CO_2$-rich pre-salt gas reservoir of the Kwanza Basin, offshore Angola

Junjie Liu [1,2,3], Honggang Zhou [4], Magali Pujol [4], David Selby [3,5], Jie Li [1,2] *, Hui Tian [2,6]

[1]State Key Laboratory of Isotope Geochemistry, Guangzhou Institute of Geochemistry, Chinese Academy of Sciences, Guangzhou 510640, China

[2]CAS Center for Excellence in Deep Earth Science, Guangzhou, 510640, China

[3]Deparment of Earth Sciences, Durham University, Durham, DH1 3LE, UK.

[4]TOTAL, Centre Scientifique et Techniques Jean-Féger, Avenue Larribau, 64018 Pau, France.

[5]State Key Laboratory of Geological Processes and Mineral Resources, School of Earth Resources, China University of Geosciences Wuhan, Wuhan, China.

[6]State Key Laboratory of Organic Geochemistry, Guangzhou Institute of Geochemistry, Chinese Academy of Sciences, Guangzhou 510640, China

* Corresponding author: Jie Li: jieli@gig.ac.cn

## Acknowledgement

We acknowledge the technical support from Ms. Antonia Hofmann, Dr. Chris Ottley, and Dr. Geoff Nowell.

## Funding

This work is supported by the National Key Research and Development Project of China (2020YFA0714800), National Natural Science Foundation of China (42003043), Total Postdoctoral research award, China Postdoctoral Science Foundation (2020M672850), Guangdong Basic and Applied Basic Research Foundation (Guangdong-Guangzhou Joint Fund; 2019A1515110310), and Hangzhou Research Institute of Geology, PetroChina (RIPED-HZDZY-2019-JS-694) grant to Junjie Liu and the Total Endowment Fund and CUG Wuhan Dida Scholarship to David Selby. The project was also supported by the NERC Innovation award (NE/L008343/1) as part of the Oil and Gas Catalyst award scheme.

## Abstract: (300 words)

Here we present a study on the formation process and Re-Os systematics of the bitumen discovered in a $CO_2$-rich pre-salt gas reservoir, south Kwanza Basin, offshore Angola. The magmatism-derived $CO_2$ may have expanded downwards from the top of the reservoir, creating $CO_2$ concentration and temperature gradients within the reservoir, and leading to the gradients of asphaltene precipitation and thermal cracking. The heat front may have been behind the $CO_2$ front due to the heat exchange with surrounding rocks. Thus, asphaltene precipitation has likely occurred before the thermal cracking. Such bitumen formation process is consistent with the observed decreasing bitumen content and Rock-Eval Tmax with depth, and also the characteristics of the whole rock and bitumen Re and Os concentrations.

Five closely spaced bitumen samples define a Re-Os age of 116 ± 29 Ma that is identical to the timing of $CO_2$ charging and thus may indicate the timing of bitumen formation. The heterogeneous $^{187}Os/^{188}Os$ and lack of mobility of the asphaltene deposit, and the relatively low extent of thermal cracking (Tmax of 425-470 °C) may account for the lack of homogenization of the bitumen initial $^{187}Os/^{188}Os$.

Given the highly radiogenic initial $^{187}Os/^{188}Os$ (ca. 1.2-1.8) of the bitumen and limited $^{187}Os/^{188}Os$ ingrowth within the ca. 15 million years from the deposition of potential source rock (Barremian-Aptian Red and Grey Cuvo formations) to the bitumen formation, the source rock should possess a highly radiogenic initial $^{187}Os/^{188}Os$ (>1).

This is consistent with that of the equivalent lacustrine strata in the conjugated Brazilian marginal basins. Thus, the Os isotope composition indicates that the lacustrine Red and Grey Cuvo formations could be the source rock for the bitumen of the studied $CO_2$-rich pre-salt gas reservoir in the south Kwanza Basin.

Keywords: Kwanza Basin, Angola; pre-salt reservoir; $CO_2$; solid bitumen; Re-Os systematics.

Highlights: (85 characters including space)

1) Magmatism-derived $CO_2$ induced asphaltene precipitation and thermal cracking.
2) Closely-spaced bitumen defines a ca. 116 Ma Re-Os age for the bitumen formation.
3) $^{187}Os/^{188}Os$ supports the lacustrine Red Cuvo Formation as the source of bitumen.
4) Bitumen $^{187}Os/^{188}Os$ show little to no influence from hydrothermal activities.

Keywords: Kwanza Basin, Angola; pre-salt reservoir; $CO_2$; solid bitumen; Re-Os systematics.

## 1. Introduction

Solid bitumen is evidence of the prior existence of crude oil. It is the remnant of crude oil alteration processes including but not limited to deasphalting and thermal cracking (Behar et al., 1991; Jacob, 1989; Meyer and De Witt, 1990; Rogers et al., 1974; Wu et al., 2000). The Re-Os geochronometer has been used to provide timing constraints for bitumen formation (Corrick et al., 2020; Corrick et al., 2019; Ge et al., 2021; Ge et al., 2018a; Ge et al., 2016; Ge et al., 2018b; Georgiev et al., 2019; Huang et al., 2018; Scarlett et al., 2019; Selby et al., 2005; Selby and Creaser, 2005; Shi et al., 2016; Su et al., 2020; Wang et al., 2019; Wang et al., 2017). Additionally, the Os isotope composition has been used to trace the source rock for crude oil and bitumen (Corrick et al., 2019; Cumming et al., 2014; Finlay et al., 2011, 2012; Ge et al., 2018a; Liu et al., 2018; Scarlett et al., 2019; Selby et al., 2005).

Here we present a study investigating the bitumen formation process in a $CO_2$-rich pre-salt gas reservoir, southern Kwanza (Benguela) Basin, offshore Angola. The solid bitumen is probably formed in response to the charge of magmatism-derived $CO_2$

during the Early Cretaceous South Atlantic Ocean opening. Organic geochemistry characterization and Re-Os analysis were conducted to constrain the nature and timing of bitumen formation and trace the source rock.

## 2. Geological background

The reservoir in this study is in the southern Kwanza (Benguela) Basin, offshore Angola (Figure 1). The Early Cretaceous pre-salt sequences of the conjugated Brazilian and Angolan continental marginal basins are characterized by continental deposits in a series of intracratonic basins in the context of the Gondwana supercontinent breakup and South Atlantic Ocean opening (Ceraldi and Green, 2017; Karner and Gambôa, 2007; Quirk et al., 2013; Saller et al., 2016; Serié et al., 2017; Torsvik et al., 2009). The lacustrine organic-rich strata that developed in the syn-rift half-grabens and sags are considered as hydrocarbon source rocks (Brownfield and Charpentier, 2006; Burwood, 1999; Pasley et al., 1998; Saller et al., 2016; Serié et al., 2017; Uncini et al., 1998). Overlying fluvial and lacustrine sandstone and carbonate units serve as reservoir rocks (Miguel et al., 2017) and they are sealed by a thick salt layer (Quirk et al., 2012).

For the studied area, the reservoir is the Chela Formation carbonate that is sealed by the Aptian Loeme Formation salt. The Barremian-Aptian Red and Grey Cuvo formations underlying the Chela Formation are the possible hydrocarbon source rocks of the Red and Grey Cuvo formations (Figure 2). The Red Cuvo Formation siliciclastic rocks possess a mix of sapropelic organic matter, scarce anisotropic bitumen and coaly fragments of terrestrial land plant debris (Type I-III kerogen; Figure 2). The average initial TOC (Total Organic Carbon) content is 2.2-2.7 wt.% and the vitrinite reflectance is 1.69-2.14%. The Grey Cuvo Formation is composed of carbonated and argillaceous siltstones and possesses Type III kerogen (Figure 2) with an average TOC content of 0.74 wt.% and vitrinite reflectance of 1.45-1.52%. Source rock maturation and oil generation may have occurred shortly after the deposition of the Barremian-Aptian source rock in response to the rapid and thick salt deposition (Saller et al., 2016; Schoellkopf and Patterson, 2000) and/or a high thermal gradient due to continental crust thinning and active magmatism during the opening of the South Atlantic Ocean.

There are often $CO_2$-rich gas traps in association with petroleum accumulations in the pre-salt sections of the conjugated Brazilian and Angolan basins on the passive continental margins (Comin-Chiaramonti et al., 2011; Foulger, 2018; Gamboa et al., 2019; Jerram et al., 2019; Melankholina and Sushchevskaya, 2018; Teboul et al., 2017). The breakup of the Gondwana supercontinent was associated with extensive magmatic activity (Figure 1; Comin-Chiaramonti et al., 2011; Jerram et al., 2019; Masse and Laurent, 2016). Magmatism-associated $CO_2$ released after the deposition of the Late Aptian salt layer can be trapped in the pre-salt reservoirs (Gamboa et al., 2019; Szatmari and Milani, 2016). The fluid of the studies reservoir consists mainly of $CO_2$ (ca. 83%) and $CH_4$ (ca. 16%). There are mainly three magmatic episodes identified in the study area (Denis and Kluska, 2017). Except for the earliest Paraná-Etendeka igneous province, two of them postdate the deposition of the Late Aptian Loeme Formation salt, i.e., the Late Aptian episode of tholeiitic magmatism during the syn- to early post-rift phase of South Atlantic Ridge breakup (Denis and Kluska, 2017; Jerram et al., 2019; Marsh and Swart, 2018; Marzoli et al., 1999; Quirk et al., 2013; Teboul et al., 2019) and a later (ca. 90 Ma) alkaline magmatic activity linked to the Sumbe Ridge activity (Denis and Kluska, 2017; Jerram et al., 2019; Marzoli et al., 1999). The $\delta^{13}C$ of $CO_2$ (-3.9‰) and the associated He signature ($R/R_a$ of 4.5 and $CO_2/^3He$ ratio of 1.2 x $10^9$) indicate that the $CO_2$ is associated with mid-ocean ridge basalt (MORB) type magmatism which is consistent with both possible magmatism episodes. The enrichment of radiogenic $^4He$ indicates that the $CO_2$ is possibly originated from the older syn- to early post-rift Late Aptian tholeiitic magmatic activity. It may have been charged into the studied reservoir through the deeply rooted fault system (Figures 1 and 5). The $CH_4$ is mainly thermogenic in origin according to its $\delta^{13}C$ of ca. -32‰ and $\delta D$ of ca. -130‰.

## 3. Samples and analytical protocol

### 3.1. Organic geochemistry characterization

The organic geochemistry characterization of the Chela Formation samples was carried out at the TOTAL CSTJF facilities in Pau, France. Maceral identification of the Chela Formation carbonates and the Grey and Red Cuvo formations was undertaken on sidewall core samples (Table 1; Figure 2) using a LEICA DM6000M microscope. Bitumen and vitrinite reflectance were determined using a LEICA CTR

6000 photometry system and Diskus-Fossil software in the random mode under reflected white incident light in oil immersion. The sidewall core samples were also measured for their Tmax and TOC contents with Rock-Eval 6 after removing the soluble oil fractions and possible drilling mud with pentane (Table 1).

### 3.2. Extraction of soluble bitumen and progressive precipitation test

Initially, three samples composed of 150 g of cuttings collected from different depths were selected to proceed to bitumen extraction followed by ASCI measurement (Asphaltene Solubility Class Index; Table 2). The first part of the protocol is to fully extract the precipitated asphaltenes from the cuttings, also called soluble bitumen, which is realized using a Dionex ASE 350 (Accelerated Solvent Extraction) from Thermo Fisher Scientific. The first step with ASE was to wash the cuttings in pure pentane under 140°C and 100 bars (3 times 3 minutes of immersion in the solvent), to remove residues of oil and drilling mud. At the end of this step, the remaining organic matter in cutting is only composed of precipitated asphaltenes and pyrolyzed bitumen. Then, the second ASE step was to use dichloromethane ($CH_2Cl_2$, DCM) solution under 100°C and 100 bars (3 times 3 min of immersion in the solvent) to extract the DCM-soluble fractions which were used for ASCI determination. Finally, solid residues were analyzed with Rock-Eval 6 to obtain the TOC corresponding to the insoluble part of bitumen which is largely pyrobitumen. Results are reported in Table 2.

The Asphaltene Solubility Class Index (ASCI) expresses the precipitation capability of the asphaltenes which can be determined for both crude oil and asphaltene deposits (Zhou et al., 2012). The aim of this classification method is to compare asphaltenes, the main component of the initial bitumen, based only on their solubility class. An asphaltene solubility class evolution with depth gives information related to the precipitation process. The workflow for ASCI determination followed the one described in Zhou et al. (2012). The determination of the ASCI begins with the preparation of 20 vials filled with 4 ml of a mix of toluene – *n*-heptane (*n*-$C_7$) with a variable ratio of the two components, covering compositions from 100wt.% Toluene to 100wt.% *n*-$C_7$ (Figure 3). Toluene is one of the best solvents for asphaltenes whereas *n*-$C_7$ is one of the best precipitants, thus variable ratios of these components lead to variable precipitation efficiency. A mark from 0, for the 0% *n*-$C_7$ and 100%

toluene solution, to 20, for the 100% *n*-$C_7$ and 0% toluene solution, is given to each vial as represented in Figure 3. Then, a few drops (3-4) of the extract are added into each vial. After that, vials are well mixed and baked for 48 hours under 50°C. Finally, there is an optical check of the presence of a precipitate and the lowest number of the vial containing a precipitate is the mark reported for the ASCI.

The asphaltene amount obtained from the 5430-5475 m interval was insufficient for ASCI determination, so it was replaced by a larger sample (500 g of crushed cuttings) covering a wider depth (5422 down to 6015 m) in order to compensate for a low asphaltene content.

### 3.3. Re-Os analyses

Complete and clean separation of bitumen from the Chela Formation carbonates is difficult to achieve either manually from the millimeter scale pores or through solvent extraction given that most of the bitumen is insoluble in the sample suite (Table 2). The fact that the Chela Formation rocks contain no autochthonous organic matter (Section 4.1) indicates that the dominant host of Re and Os in the Chela Formation reservoir rock is the bitumen. Thus, bitumen Re-Os systematics was analyzed using whole rock powder instead. The Re and Os concentrations of bitumen were approximately determined using the TOC contents of the whole rock.

The Re-Os analyses were conducted by Isotope Dilution-Negative Thermal Ionization Mass Spectrometry (ID-NTIMS) on eleven Chela Formation whole rock bitumen bearing samples (Table 3) at the Durham Geochemistry Centre at Durham University in the Laboratory for Source Rock and Sulphide Geochronology and Geochemistry and the Arthur Holmes Laboratory. Following the procedures described in Selby et al. (2007a) and Liu and Selby (2018), approximately 200 mg of the bitumen bearing whole rock powder for each sample was placed into a Carius tube together with a mixed tracer solution of $^{185}Re$ and $^{190}Os$ and then digested and equilibrated in inverse *aqua regia* (3 ml 12 N HCl + 6 ml 15.5 N $HNO_3$) at 220 °C for 24 h. The Os was extracted from the acid solution using chloroform and back-extracted with 3 ml of 9 N HBr. The Os fraction was further purified by micro-distillation using $CrO_3$-$H_2SO_4$ and HBr. The Re was purified from the dried acid solution by NaOH-solvent extraction and HCl-$HNO_3$ based anion exchange chromatography. The purified Re and Os

fractions were loaded on Ni and Pt filaments, respectively, and measured for their isotopic compositions by NTIMS using static collection by Faraday cups for Re and peak-hopping mode on a secondary electron multiplier for Os. The total procedural blanks during the study are 1.63 ± 0.67 picograms for Re and 65 ± 13 femtograms for Os, with an average $^{187}Os/^{188}Os$ of 0.23 ± 0.02 (2 SD, n = 8). IsoplotR (Vermeesch, 2018) is used to derive all Re-Os isochron dates through statistical regression of the Re-Os data, which are reported at the 2σ level (95% level of confidence), in $^{187}Re/^{188}Os$ vs. $^{187}Os/^{188}Os$ space using the decay constant of $^{187}Re$ of $1.666e^{-11}$ ± $5.165e^{-14}$ $a^{-1}$ (Smoliar et al., 1996).

# 4. Results

## 4.1. The organic geochemistry of the Chela Formation carbonates

The only organic matter observed in the Chela Formation carbonate is pore-filling anisotropic bitumen exhibiting undulose extinction. There is no autochthonous organic matter observed. The crude oil fractions extracted by pentane may contain drilling mud and thus is not further discussed. The TOC contents measured on pentane-washed samples are used here to represent the bitumen contents which decrease with depth almost exponentially from a maximum of 4.50 wt.% at 5303 m to a minimum of 0.38 wt.% at 5494 m (Table 1; Figure 4a). Such bitumen consists of mainly (ca. 87-97%) the DCM-insoluble fractions, which are largely pyrobitumen, and minor (ca. 3-13%) DCM-extracted soluble fractions, i.e., the asphaltenes (Table 2). The bitumen reflectance ($BR_o$) of the four samples from 5309 to 5494 m are 1.88-1.98% which are equivalent to vitrinite reflectance ($VR_o$) of 1.56-1.62% (Table 1; Figure 4b; Jacob, 1989). The Rock-Eval Tmax of the Chela Formation samples decreases with depth from 470 °C at 5304 m to 426 °C at 5494 m (Table 1; Figure 4c). The ASCI marks of the asphaltene of the soluble fractions extracted from the powders of 5300-5350 m, 5370-5415 m and 5422-6015 m are 7, 5 and 1, respectively (Table 2). In summary, the content (Rock-Eval TOC) and Tmax of the DCM-insoluble solid bitumen, the content and solubility (ASCI mark) of the DCM-soluble asphaltene, and thus the total content of the solid bitumen decrease with depth. However, the $BR_o$ does not show such a gradient.

### 4.2. Re-Os analyses results

The whole rock samples of Chela Formation carbonates contain ca. 0.1-3.6 ppb (parts per billion) Re and 3-100 ppt (parts per trillion) Os (Table 3). The approximate bitumen Re and Os concentrations based on the TOC (DCM-insoluble bitumen) contents of the whole rock samples are ca. 2-380 and 0.1-19 ppb, respectively (Table 3). The $^{187}Re/^{188}Os$ and $^{187}Os/^{188}Os$ of the samples are ca. 30-460 and 1.3-2.7, respectively, and they are generally positively correlated (Table 3).

## 5. Discussion

### 5.1. Bitumen formation process

The lack of fluorescence, relatively high maturity ($BR_o$ of ca. 2.0% and Tmax as high as 470 °C; Figure 4b-c; Table 1) especially for the samples above 5400m, and limited solubility (Table 2) indicate that at least part of the solid bitumen in the Chela Formation are possibly pyrobitumen formed by thermal cracking. In addition to pyrolysis, the DCM-insoluble bitumen can be also formed through the asphaltene precipitation process as will be discussed below. The small portions of pentane-soluble hydrocarbon and DCM-soluble asphaltene fractions could be the remnant of asphaltene deposit after the thermal cracking and/or the product of thermal cracking. The source of heat for the possible thermal cracking is likely to be the magmatism-originated $CO_2$ (Denis and Kluska, 2017) given its high capacity to carry and transfer energy (Hu et al., 2004; Ishmael et al., 2016) and high concentration in the reservoir fluid (ca. 83%). The bulk of the remaining gas in the reservoir is $CH_4$ (ca. 16%), which is mainly thermogenic in origin and therefore less capable of inducing the thermal cracking of crude oil.

The decrease in Rock-Eval Tmax of the Chela Formation samples may indicate that there is a decrease in thermal stress with depth within the reservoir, yet this is not apparent from the $BR_o$ data (Figure 4b-c; Table 1). The magmatism-derived hot $CO_2$ may have been charged from or accumulated at the top of the reservoir firstly through the deeply-rooted faults (Figure 1c and 5) and then expanded downwards along with its continuous charge, creating downward decreasing gradients of $CO_2$ concentration and temperature in the reservoir before the final equilibrium state (Figure 6). As a

result, the maturity of the solid bitumen can be greater in the higher positions of the reservoir given the higher temperature and longer duration of thermal cracking.

The heat front could have been far behind the $CO_2$ concentration front during the $CO_2$ charging process. In the initial stage of $CO_2$ charging, hot (600-1100 °C) $CO_2$ could have been cooled down by the surrounding rocks on its pathway because of the overwhelmingly higher heat capacity of rocks than the $CO_2$-rich fluid. Carbon dioxide has a strong ability to induce asphaltene precipitation (Gonzalez et al., 2008; Monger and Fu, 1987; Srivastava et al., 1999; Zanganeh et al., 2018). Deposits of precipitated asphaltene may have formed in response to the charge of the cooled $CO_2$. The precipitation of asphaltene from crude oil is a progressive process along with the change in condition (Zhou et al., 2012). For example, the addition of more *n*-$C_7$ into the DCM solution of asphaltene will lead to the precipitation of more asphaltene (Figure 3; DiMarzio et al., 2018; Liu et al., 2019; Mahdaoui et al., 2013; Nalwaya et al., 1999; Passade-Boupat et al., 2013; Zhou et al., 2012). Similarly, low concentration $CO_2$ can only induce the precipitation of highly unstable asphaltene species from crude oil while higher concentration $CO_2$ could induce more asphaltene to precipitate. In response to the upward increasing $CO_2$ concentration, there could have been more asphaltene precipitated in the higher position of the reservoir (Figure 5-6). This proposed asphaltene precipitation process is consistent with the decreasing total bitumen contents with depth within the reservoir (Table 1; Figure 4). A large volume of $CO_2$ is required to warm up the pathway rock. Before the $CO_2$ influx into the reservoir became hot, the mobile fractions of crude oil may have been driven away from the reservoir and have not been involved in the following thermal cracking processes. Thus, the current content of organic matter in the reservoir could have been largely determined by the precipitated asphaltene, although it may have been slightly altered by the subsequent thermal cracking.

Once the surrounding rock on the pathway was warmed up, the hot $CO_2$ injected into the reservoir could lead to the thermal cracking of the precipitated asphaltene. Similarly, due to the heat exchange with the reservoir rock, the $CO_2$ may have been cooled down quickly in the reservoir thus creating a temperature gradient in the reservoir. The downward decreasing temperature gradient may have created correspondingly decreasing maturity of the solid bitumen as indicated by Tmax. The

pyrobitumen yield can be higher in the higher positions of the reservoir from the asphaltene deposit under a higher degree of thermal cracking, e.g., with the Tmax as high as 470 ℃. The laboratory experiment of Lei et al. (2018) shows that the percentages of pyrobitumen in the pyrolysate from asphaltene plus resin increase with maturity, which are ca. 20, 40 and 50% at Easy$R_o$ of 1.0, 1.5 and 2.2%, respectively, to be specific. The maximum pyrobitumen yield is ca. 60% with the remaining pyrolysate to be mainly methane at Easy$R_o$ of up to 5.0% (Lei et al., 2018). In contrast, the Tmax is under 435 °C below 5400 m indicating a relatively low extent of thermal cracking and thus a low yield of pyrobitumen. However, there is still more than 87% of the solid bitumen insoluble in DCM below 5400 m (Table 2).

The $BR_o$ may not be the best indicator for the thermal maturity of the bitumen deposit in this study. According to Nalwaya et al. (1999), the asphaltene precipitated in different stages, i.e., with different ASCIs, may have different physical appearance and macrostructure properties. The ones that precipitate earlier with lower ASCIs are hard, shiny and dense black particles having planar surfaces while the ones that precipitate later with higher ASCIs are soft, dull and brown powder and appear as porous and undefined structures under the scanning electron microscope (Nalwaya et al., 1999). This may lead to different optical properties, i.e., higher reflectance ($BR_o$) for the bitumen with lower ASCIs even if all the bitumens have totally the same thermal history. However, no molecular weight nor functional group differences have been observed among the progressively precipitated fractions of asphaltene (Nalwaya et al., 1999). This probably means that the Rock-Eval Tmax may remain unchanged. In fact, the Rock-Eval Tmax has long been used as a thermal maturity indicator within the immature to wet gas window (Behar et al., 2001; Evenick, 2021; Katz and Lin, 2021; Lafargue et al., 1998; Nali et al., 2000; Rahman and Rimmer, 2014; Rahman et al., 2018; Rahman et al., 2017a; Rahman et al., 2017b; Yang and Horsfield, 2020). Prior to the thermal alteration, the asphaltene precipitates formed through progressive process deposits in the studied reservoir may show an increase of reflectance ($BR_o$) with depth in response to a decreasing ASCI but constant Tmax. In fact, the $BR_o$ and Tmax at the top of the reservoir are higher than this expectation, indicating the higher extent of thermal alteration than the lower part of the reservoir and thus supporting the bitumen formation model proposed in this study (Figure 5-6).

The ASCI evolution shows that the deeper the sample is, the lower solubility is for its DCM-extracted asphaltene in the mixture of *n*-$C_7$ and toluene (Table 2). An important fact about asphaltene is that the unstable asphaltene species can be stabilized by the presence of the relatively more stable asphaltene species in crude oil and solutions given their strong interaction (Zhou et al., 2012). As a result, the ASCI mark determined for the asphaltene deposit is lower than that for its original crude oil due to the lack of support from the relatively more stable asphaltene species. Meanwhile, among the asphaltene deposits precipitated from the same crude oil, the ones precipitated from worse solvents (e.g., mixtures of higher *n*-$C_7$ to toluene ratio or higher concentrations of $CO_2$) with higher asphaltene yields will have higher ASCI mark than the ones precipitated from better solvents (e.g., mixtures of lower *n*-$C_7$ to toluene ratio or lower concentrations of $CO_2$) because of the co-precipitation of the more stable asphaltene species. Thus, before the thermal cracking, the asphaltene deposits in the studied reservoir may have had a decreasing ASCI mark gradient with depth as a result of the decreasing $CO_2$ concentration gradient. The current DCM-extracted asphaltenes are the remnant of asphaltene deposits after the thermal cracking and/or the product of thermal cracking. Nevertheless, they still show a decrease in ASCI marks from 7 to 1 with depth, meeting the expectation for the asphaltene deposit according to the proposed bitumen formation process.

The insolubility of the bitumen with low Tmax could be related to the deasphalting process. The DCM-insoluble bitumen can be formed through not only pyrolysis but also the asphaltene precipitation process. For example, the solid bitumens from the Mitsue Field, Canada formed through geological gas deasphalting with $BR_o$ of ~0.7% are not fully soluble in organic solvents (Hwang et al., 1998). One of such bitumen has 14.7%, 46% and 20% extracted by cyclohexane, DCM and toluene, respectively, with 19.3% remaining insoluble. For the DCM-extract of the lowest 5422-6015 m sample in this Angolan reservoir, the ASCI of 1 indicates that it has asphaltene fractions that are insoluble in the mixture of 95% toluene and 5% *n*-heptane but soluble in pure toluene and DCM (Figure 3). There may be asphaltene fractions with even lower solubility, i.e., ASCI of 0, which precipitated under low $CO_2$ concentration and cannot be redissolved or extracted by the DCM-ASE practice due to the absence of support from the more soluble asphaltene species in crude oil.

In other reservoirs of the Kwanza Basin and conjugated Brazilian Campos and Santos basins, it is suggested that geothermal fluids led to the thermal cracking of crude oil and bitumen formation (Girard and Miguel, 2017; Girard and Miguel, 2018; Girard et al., 2017; Loma et al., 2018; Tritlla et al., 2019; Tritlla et al., 2018). Paleo fluid reconstructions on the ultra-stretched domain of the Kwanza Basin indicate that a hot (197-221 °C) saline hydrothermal plume telescoped a liquid oil reservoir and thermally cracked the oil into pyrobitumen and wet gas (Loma et al., 2018; Tritlla et al., 2019; Tritlla et al., 2018). An integrated diagenetic study on a well in the southwestern Kwanza Basin near the Benguela Transfer Fault Zone also demonstrates that the pre-salt reservoir was heated to unusually high temperatures (> 150 °C) shortly after deposition (within 15-20 million years) according to fluid inclusion analysis and affected by profound hydrothermal diagenesis driven by $CO_2$-rich highly saline brines (Girard and Miguel, 2017; Girard and Miguel, 2018; Girard et al., 2017). Unfortunately, there are no details on hydrothermal fluid activity in the area of the studied reservoir. Nevertheless, little to no influence of the hydrothermal activities on the bitumen Os isotope composition of the reservoir has been identified in this study (see below). If Tmax can be considered as a reliable parameter to compare the thermal cracking extent of bitumen, its decrease with depth could be hardly explained by the thermal cracking induced by hydrothermal fluids.

In summary, the bitumen in the studied reservoir was probably formed sequentially through the asphaltene precipitation and the thermal cracking processes induced by the magmatism-derived $CO_2$. The charged hot $CO_2$ may have been cooled down by the pathway rocks initially before the rocks were warmed up. The $CO_2$ may have expanded downwards from the top of the reservoir and thus leading to the formation of more bitumen through asphaltene precipitation in the higher positions of the reservoir. The later hot $CO_2$ led to the thermal cracking of the asphaltene deposit. The DCM-insoluble bitumen could contain both the pyrobitumen and precipitated asphaltene with low solubility. The downward decreasing gradients of the total contents of the DCM-soluble and insoluble bitumen, Tmax and ASCI marks are consistent with the proposed bitumen formation model.

## 5.2. Bitumen Re-Os concentration characteristics and implications

Overall, the Os (represented by the most abundant stable isotope $^{192}Os$) concentrations of the bitumen-bearing reservoir rock samples decrease with depth in the studied reservoir (Table 3; Figure 7). The bitumen $^{192}Os$ concentrations determined based on the TOC contents of the solvent-extracted rocks generally increase with depth (Table 3; Figure 7). These observed trends can be accounted for by the bitumen formation processes and the residency of Os in crude oil fractions (DiMarzio et al., 2018; Georgiev et al., 2016; Georgiev et al., 2019; Hurtig et al., 2020; Liu and Selby, 2018; Liu et al., 2019; Mahdaoui et al., 2013; Selby et al., 2007a; Stein and Hannah, 2016).

It has been demonstrated that the crude oil Re and Os are predominantly hosted by the asphaltene fraction rather than the maltene fraction (DiMarzio et al., 2018; Georgiev et al., 2016; Georgiev et al., 2019; Hurtig et al., 2020; Liu and Selby, 2018; Liu et al., 2019; Selby et al., 2007a; Stein and Hannah, 2016). Further analyses showed that the Re and Os of maltene concentrate in the resin fraction, with only very limited Re and Os in the aromatic and saturated hydrocarbons (DiMarzio et al., 2018). It is also demonstrated by the asphaltene sequential precipitation experiments that the fractions of asphaltene which precipitate earlier from the binary mixture solvents with increasing precipitant content, i.e., the ones with lower ASCI marks, generally have higher Re and Os concentrations (DiMarzio et al., 2018; Liu et al., 2019; Mahdaoui et al., 2013).

In the lower position of the studied reservoir, the asphaltene deposits had lower ASCI marks as they were precipitated under lower $CO_2$ concentrations. Thus, they may have higher Os concentrations than the ones precipitated in higher positions. The whole rock's Os concentrations are related to the bitumen contents – the precipitation of more asphaltene will enhance the Os contents and thus concentrations in the whole rock in the higher position of the studied reservoir. Although the Re-Os systematics may have been altered by the subsequent thermal cracking of the asphaltene deposits (Ge et al., 2021; Ge et al., 2016; Ge et al., 2018b; Lillis and Selby, 2013), there are still signs of such Os concentration characteristics of the bitumen and whole rock in the studied reservoir (Table 2; Figure 7).

The same could have also been true for the Re, however, most of the bitumen Re concentrations are within 150 ppb showing no significant trends (Table 3; Figure 7). An increase with depth is only shown between 5300 and 5400 m which is strongly controlled by the sample PRA6.

## 5.3. Re-Os bitumen geochronology, Kwanza Basin

The Re-Os isochron dates obtained from low maturity bitumen are interpreted as oil generation age (Corrick et al., 2019; Cumming et al., 2012; Cumming et al., 2014; Ge et al., 2020; Ge et al., 2018a; Ge et al., 2016; Huang et al., 2018; Scarlett et al., 2019; Selby et al., 2005; Selby and Creaser, 2005). In contrast, the Re-Os systematics in highly mature bitumen are interpreted to record the cessation timing of their formation through thermal cracking (Ge et al., 2021; Ge et al., 2016; Ge et al., 2018b; Lillis and Selby, 2013).

The Re-Os data of all samples in this study define an *IsoplotR* Model 3 isochron age of 174 ± 37 Ma (n = 11; initial $^{187}Os/^{188}Os$ ($Os_i$) = 1.44 ± 0.14; Figure 8a). The age of ca. 174 Ma is older than the overall chronology of the petroleum system. The source rock is the Barremian-Aptian Red and Grey Cuvo formations (ca. 125 ~ 130 Ma; Burwood, 1999; Ceraldi and Green, 2017; Coward et al., 1999). The start of the Loeme Formation seal deposition and thus the earliest possible oil accumulation is ca. 117 Ma (Quirk et al., 2013). The charge of magmatic-sourced $CO_2$ which induced bitumen formation occurred during the Late Aptian (Denis and Kluska, 2017). The presence of bitumen indicates that there has been oil charged into the studied Chela Formation carbonate reservoir. The pre-salt section source rocks may have become mature soon after the deposition due to the abnormally high thermal regime as a result of the continental crust thinning and magmatism during the South Atlantic Ocean opening (White et al., 2003) and/or in response to the rapid and thick salt deposition (Saller et al., 2016; Schoellkopf and Patterson, 2000). Danforth (1998) also suggested that they entered the oil window since the Early Paleogene which is not supported by this study.

Samples possessing a range in $^{187}Re/^{188}Os$ and identical initial $^{187}Os/^{188}Os$ ($Os_i$) are prerequisites for dating via the isochron approach. The elevated MSWD of 7.8 for the best-fit of all the data proposes that there is scatter about the best-fit line beyond that

associated with analytical uncertainty. An apparent reason for the scatter is the variation in $Os_i$ of the samples in this study, which are 1.18-1.65 and 1.24-1.79 when calculated at 174 and 117 Ma, respectively (Table 3). The best-fit of the data using *IsoplotR* states the variation in initial $^{187}Os/^{188}Os$ is 0.069 to 0.199 at 174 Ma (Figure 8a; Vermeesch, 2018). Further, the scatter about the best-fit line can also be partially controlled by the limited spread in the $^{187}Re/^{188}Os$ of the sample suite (Table 3).

Variation in the initial $^{187}Os/^{188}Os$ has also been observed for pyrobitumen samples from previously studied petroleum systems, which results in high levels of scatter about the best-fit line and imprecise Re-Os ages although in nominal agreement with the petroleum evolution history of the given basins (Ge et al., 2021; Ge et al., 2016; Ge et al., 2018b). For example, pyrobitumen of the Xuefeng uplift, southwestern China with $BR_o$ > 2% and Tmax > 550 ℃ and a sample spacing of tens of kilometers show a $^{187}Re/^{188}Os$ range of ca. 90-500 with initial $^{187}Os/^{188}Os$ ($Os_i$) of 1.29-1.54 (Ge et al., 2016); pyrobitumen from the Micang Shan uplift, southwestern China with $BR_o$ of 3-4% and a sample spacing of a few kilometers exhibit a $^{187}Re/^{188}Os$ range of ca. 160-340 and $Os_i$ of 2.0-2.5 (Ge et al., 2018b); and pyrobitumen from the outcrops of Nanpanjiang Basin, southern China with $BR_o$ > 2% with a sample spacing of 3 meters to tens of kilometers have a $^{187}Re/^{188}Os$ range of ca. 68-683 and $Os_i$ of 0.17-0.56 (Ge et al., 2021).

The calculated $Os_i$ of a suite of bitumen samples can be heterogeneous if they are not formed contemporaneously, the Re-Os systematics have been disturbed after the formation, or the bitumen formation process does not completely homogenize the heterogeneous $^{187}Os/^{188}Os$ of the source (Davies et al., 2018; Ge et al., 2021; Lillis and Selby, 2013). Given that the bitumen in the studied reservoir is considered to have formed contemporaneously via the charge of magmatism-derived $CO_2$ and there is no evidence for post-formation alteration of the bitumen, it is probably the bitumen formation process, i.e., firstly the asphaltene precipitation and then the thermal cracking, that is responsible for the incomplete homogenization of $^{187}Os/^{188}Os$. This may directly relate to the incomplete transformation of crude oil into pyrobitumen.

The progressively precipitated fractions of asphaltenes of some crude oil samples in previous studies have similar $^{187}Os/^{188}Os$ while some other samples do not (DiMarzio et al., 2018; Liu et al., 2019; Mahdaoui et al., 2013). The fractions of the asphaltenes

of RM 8505 even define an Isoplot Model 1 Re-Os age close to the deposition age of possible source rock (Liu et al., 2019). As the calculated $Os_i$ of the bitumen in this study is heterogeneous, the asphaltene deposits may have had heterogeneous $^{187}Os/^{188}Os$.

Thermal cracking may alter the Re-Os systematics of crude oil and even reset the Re-Os geochronometer (Ge et al., 2021; Ge et al., 2016; Ge et al., 2018b; Lillis and Selby, 2013). According to the agreement of apatite fission-track (AFT) and pyrobitumen Re-Os ages of the Xuefeng Uplift, China, it is inferred that the closure temperature range of hydrocarbon Re-Os systematics is similar to that of AFT, i.e., 120-60 °C (Ge et al., 2016; Kohn and Green, 2002). However, it is poorly understood how heterogeneous $^{187}Os/^{188}Os$ composition is homogenized during the pyrobitumen formation from both the asphaltene deposit in this study and the crude oil. The controlling factors for the diffusion of Os may include the mobility of the organic matter, the temperature and duration of the thermal cracking, the distance, and possibly the residence of Os in crude oil, etc. Firstly, the asphaltene deposit in this study is not as mobile as crude oil and thus the Os diffusion can be relatively difficult. Secondly, the maturity of the bitumen (Tmax of 425-470 ℃ and $BR_o$ equivalent $VR_o$ of ca. 1.6%) is not as high as that of the previous studies (e.g., Tmax > 550 ℃ and BRo > 2%; Ge et al., 2021; Ge et al., 2016; Ge et al., 2018b). The bitumen samples are not wholly pyrobitumen as there is still a soluble fraction consisting of the remnant of asphaltene deposit after the thermal cracking and/or the product of thermal cracking (Table 2) and the possible progressively precipitated asphaltene fractions with very low solubility as discussed in Section 5.1. The Tmax of the bitumen decreases with depth – it is below 435 and 431 ˚C for samples below 5400 m and 5430 m, respectively, indicating a relatively low extent of thermal cracking in the lower part of the reservoir as noted before (Figure 4; Table 1). Thus, the bitumen maturity is probably not high enough for the thorough homogenization of $^{187}Os/^{188}Os$ over a vertical distance of ca. 200 m in the studied reservoir.

The degree of fit of the Re-Os isochron defined by samples with heterogeneous $Os_i$ can be evaluated by assessing the deviation of all the data points from the best-fit line (Ge et al., 2018b; Kendall et al., 2004; Rooney et al., 2011; Selby and Creaser, 2003). Samples PRA9 and 10 (-16 and -6%, respectively, Figure 8a) show the greatest

deviation from the best-fit of all the Re-Os data defining a ca. 174 Ma age. This overdispersion is supported by the inverse isochron approach which utilizes the Re-Os data in $^{188}Os/^{187}Os$ vs $^{187}Re/^{187}Os$ space (Figure 8b; Li and Vermeesch, 2021). Moreover, hierarchical clustering of the Re-Os data (Cumming et al., 2014; Lillis and Selby, 2013; Sai et al., 2020) based on calculated $Os_i$ values at the possible key geological timings, e.g., source rock deposition age of 130-125 Ma and the earliest possible timing of bitumen formation based on the age of the Loeme Formation seal (117 Ma) illustrates samples PRA9 and 10 possess largely different initial $^{187}Os/^{188}Os$ compositions. Regression of the Re-Os data without samples PRA9 and 10 yields a Model 1 Re-Os isochron age of 131 ± 21 Ma ($Os_i$ = 1.68 ± 0.11; Mean Squared Weighted Deviates [MSWD] = 0.73) that is in much closer agreement with that of the Kwanza petroleum system (Figure 8c). Although a Model 1 solution for the Re-Os data, in $^{188}Os/^{187}Os$ vs $^{187}Re/^{187}Os$ space scatter about the best-fit is defined by PRA1, 4 and 7 (Figure 8d). These samples exhibit -3.9% to -9.3% deviation from the ca. 131 Ma best-fit line in $^{187}Re/^{188}Os$ vs $^{187}Os/^{188}Os$ space (Figure 8c).

Further assessment of the best-fit of the Re-Os data defines PRA2, 3, 5, 6, and 8 to yield the best-fit of the Re-Os bitumen data, defining a Model 1 (*IsoplotR*) Re-Os isochron age of 116 ± 29 Ma and initial $^{187}Os/^{18}Os$ of 1.77 ± 0.15 (MSWD of 0.18; Figure 8e). The nominal age is identical to the timing of the Late Aptian mid-ocean ridge basalt (MORB) type magmatic activity, i.e., the charge of $CO_2$ into the reservoir (Denis and Kluska, 2017; Quirk et al., 2013), and thus, be the best estimate of the timing of bitumen formation. These adjacent bitumen samples are from a ca. 100 m interval of 5327.26-5430.19 m in the relatively high part of the reservoir where the Tmax of bitumen is higher (> 435 °C), indicating that Os isotope composition may have possibly homogenized under high temperatures across short distances or that the asphaltene deposits in this interval had homogeneous $^{187}Os/^{18}Os$ after the precipitation induced by $CO_2$.

## 5.4. Source rock tracing utilizing Os isotope compositions

Tracing the source rock for highly mature pyrobitumens is critical for the understanding of the source kitchen and migration pathway of crude oil and thus its exploration (Curiale, 2008; Shi et al., 2015). The application of the Os isotope composition to identify the source unit of hydrocarbons has been discussed for several

549 petroleum systems on the basis that crude oil inherits the $^{187}Os/^{188}Os$ of the source
550 rock at the timing of oil generation (Corrick et al., 2019; Cumming et al., 2014; Finlay
551 et al., 2011, 2012; Ge et al., 2018a; Liu et al., 2018; Rooney et al., 2012; Scarlett et al.,
552 2019; Selby et al., 2005). This is an effective oil-source tracer and it can be important
553 when the source-tracing using biomarkers and stable isotopes is hampered by the
554 biodegradation and thermal cracking of crude oil (Curiale, 2008). However, tracing
555 the source rock for pyrobitumen with Os isotope composition is more difficult than
556 for the crude oil as it involves post crude oil formation processes, e.g., thermal
557 cracking, which has been shown to reset the Re-Os radioisotope system. The possible
558 source rocks for the pre-salt hydrocarbon accumulations in the offshore Kwanza
559 Basin and the conjugated Brazilian marginal basins are the organic-rich mudstone,
560 marl, and shales deposited in the deep lacustrine environment during the Barremian to
561 Aptian syn-rift and sag stages (Brownfield and Charpentier, 2006; Burwood, 1999;
562 Ceraldi and Green, 2017; Danforth, 1998; Saller et al., 2016). The organic-rich
563 Barremian-Aptian Red and Grey Cuvo formations of the studied area are possible
564 source rock for the initial crude oil in the Chela Formation carbonate reservoir,
565 especially the thick Red Cuvo Formation (ca. 397 m) with abundant oil-prone
566 sapropelic organic matter. Although the $^{187}Os/^{188}Os$ of these formations are
567 unavailable, studies have shown that the nearly contemporaneous equivalent
568 lacustrine source rocks of the conjugated Brazilian basins are characterized by highly
569 radiogenic initial $^{187}Os/^{188}Os$ (Creaser et al., 2008; Lúcio et al., 2020).

570 The Ipubi Formation black shale of the Araripe Basin, northeastern Brazil with an
571 Early Aptian Re-Os age of 123 ± 3.5 Ma is characterized by initial $^{187}Os/^{188}Os$ of
572 1.75-2.05, suggesting that the Araripe Basin water mass was highly restricted
573 although there was a marine influence (Lúcio et al., 2020). Further south, the
574 Neocomian shales of the Sergipe-Alagoas Basin with a Re-Os age of ca. 139 Ma, the
575 shales of the Aratu chronostratigraphic local stage with a Re-Os age of ca. 131 Ma
576 and the underlying shales of the Rio da Serra local stage with a Re-Os age of ca. 140
577 Ma of the Reconcavo Basin, and the Lagoa Feia Formation of the Campos Basin
578 (Jiquia chronostratigraphic local stage) with a Re-Os age of ca. 125 Ma are
579 characterized by initial $^{187}Os/^{188}Os$ of 1.3-1.5 (Creaser et al., 2008). The Os source for
580 the lacustrine water column was predominantly continental runoff from the
581 weathering of Precambrian and Phanerozoic igneous and sedimentary rocks which

can possess a highly radiogenic $^{187}Os/^{188}Os$ composition (Creaser et al., 2008; Cumming et al., 2012; Ehrenbrink and Ravizza, 1996; Pietras et al., 2020; Poirier and Hillaire-Marcel, 2011; Xu et al., 2017). Given the lacustrine paleodepositional setting for the Red and Grey Cuvo formations of the Kwanza Basin coupled with the presence of terrestrial organic matter input (Burwood, 1999; Serié et al., 2017; Uncini et al., 1998) the hydrogenous $^{187}Os/^{188}Os$ is considered to have been highly radiogenic.

Based on the timing of the tholeiitic magmatic activity as the source for the $CO_2$ (Late Aptian; Denis and Kluska, 2017) and the Re-Os geochronology (116 ± 29 Ma), the bitumen in the studied reservoir formed shortly after the deposition of the potential source rock, i.e., the Barremian-Aptian Red and Grey Cuvo formations (ca. 129.4 Ma onwards; Cohen et al., 2013). The source rocks may have entered the oil window soon after their deposition due to the deposition of the thick salt layer (Saller et al., 2016; Schoellkopf and Patterson, 2000) and/or high thermal gradient due to continental crust thinning and active magmatism during the opening of the South Atlantic Ocean. Thus, radiogenic ingrowth of $^{187}Os/^{188}Os$ from the radiometric decay of $^{187}Re$ is considered to have limited from source rock deposition to bitumen formation considering the long half-life of $^{187}Re$ (ca. 41.6 billion years; Selby et al., 2007b; Smoliar et al., 1996). Assuming a $^{187}Re/^{188}Os$ as high as 1000 for both the source rock and crude oil based on the Re-Os data of the Ipubi Formation black shale of the Araripe Basin, northeastern Brazil (highest $^{187}Re/^{188}Os$ of 876; (Lúcio et al., 2020), and the bitumen in this study (highest $^{187}Re/^{188}Os$ of 462), the $^{187}Os/^{188}Os$ can increase by 0.25 in 15 million years. Given that the source rock for the crude oil is considered to possess $^{187}Os/^{188}Os$ values > 1 at its deposition, the initial $^{187}Os/^{188}Os$ of 1.24-1.80 for the bitumen samples at 116 Ma is consistent with the possibility that the crude oil was sourced from the lacustrine units of the Red and Grey Cuvo formations.

## 5.5. Hydrothermal fluid influence on the $^{187}Os/^{188}Os$ of bitumen

Pervasive hydrothermal diagenesis has been discovered in the pre-salt Aptian lacustrine carbonates of the conjugated Campos and Santos basins of Brazil and the Kwanza Basin of Angola along the South Atlantic margins (Girard and Miguel, 2017; Girard and Miguel, 2018; Girard et al., 2017; Loma et al., 2018; Saller et al., 2016; Teboul et al., 2019; Tritlla et al., 2019; Tritlla et al., 2018) and there is the argument

that the geothermal fluids may have induced the thermal cracking of crude oil and formation of solid bitumen in a Kwanza Basin reservoir (Tritlla et al., 2018).

Laboratory experiments demonstrate that the aqueous Re and Os can be transferred to crude oil and alter the Re-Os systematics of crude oil (Hurtig et al., 2019; Mahdaoui et al., 2015). The crude oils spatially associated with the main basin-bounding faults of the Viking Graben and East Shetland Basin of the North Sea, United Kingdom were also shown to have an unradiogenic Os isotope composition caused by the interaction of mantle-derived fluids (Finlay et al., 2010). Hydrothermal fluids associated with the magmatic activities during the opening of the South Atlantic Ocean or by migrating through thick volcanic intervals in the South Atlantic Ocean marginal basins (Saller et al., 2016) could have resulted in lowering the $^{187}Os/^{188}Os$ of any present hydrocarbons to a more mantle-like $^{187}Os/^{188}Os$ of ca. 0.12-0.13 (Faure, 1986; Meisel et al., 2001). However, the bitumen $^{187}Os/^{188}Os$ are much more radiogenic in this study (> 1.2; Table 3), indicating that the hydrothermal activity contributes little to no Os to the solid bitumen in this study or that hydrothermal activity may have never been involved in the bitumen formation and post-formation alteration processes in the studied reservoir. Similarly, it is observed that basinal fluids have little to no influence on the $^{187}Os/^{188}Os$ of the crude oils in the Devonian Leduc and Nisku carbonate reservoirs (Liu et al., 2018). Also, the aqueous Os may have only been transferred to the bitumen in the first contact with the hydrothermal fluid and such bitumen was not sampled.

## 6. Conclusion

The studied pre-salt gas reservoir of offshore Kwanza Basin, Angola is rich in magmatism-derived $CO_2$ and bitumen. Vertical decreasing gradients of the maturity (Rock-Eval Tmax) and content of bitumen, as well as the asphaltene solubility (ASCI mark) of the soluble bitumen fraction, are observed in this reservoir.

A model is proposed for the bitumen formation process whereby magmatism-originated $CO_2$ was initially charged from or accumulated at the top of the reservoir and then expanded downwards along with the continuous charge, creating vertical decreasing $CO_2$ concentration and temperature with depth. These gradients led to the formation of more bitumen through a higher degree of asphaltene

precipitation and thermal cracking in the higher position of the reservoir, thus creating the content and maturity gradients of bitumen in the reservoir. The asphaltene precipitation may have occurred earlier than the thermal cracking as the heat front could be behind the $CO_2$ front – the $CO_2$ may have been cooled down by the surrounding rock on its pathway in the first stage and led to the precipitation of asphaltene in the reservoir. Once the surrounding rock was warmed up, the $CO_2$ charged into the reservoir became hot and may have induced the thermal cracking of the asphaltene deposit. Meanwhile, the variation of the bitumen Re and Os concentrations is also consistent with such bitumen formation process and the residence of the Re and Os in crude oil.

The calculated initial $^{187}Os/^{188}Os$ of the bitumen samples at the key timings of the reservoir, e.g., the $CO_2$ charging and bitumen formation (ca. 116 Ma), are heterogeneous. This indicates that the bitumen formation processes were incapable of homogenizing the $^{187}Os/^{188}Os$ on the scale of vertically ca. 200 m in the studied reservoir. The asphaltene deposits may have been formed with heterogeneous $^{187}Os/^{188}Os$. The controlling factors for the $^{187}Os/^{188}Os$ homogenization during the pyrobitumen formation process are possibly the mobility of the organic matter, maturity level and distance. Five samples from a ca. 100 m interval of 5327.26-5430.19 m, a zone of relatively high Tmax, are found to have the most proximate initial $^{187}Os/^{188}Os$ among the samples according to hierarchical clustering. They define a Re-Os age of 116 ± 29 Ma which is identical to the timing of $CO_2$ charging and thus may indicate the formation of the bitumen.

The very radiogenic initial $^{187}Os/^{188}Os$ of the bitumen and the short duration from source rock deposition to bitumen formation indicate that the source rock should have highly radiogenic initial $^{187}Os/^{188}Os$ as well (>1). This is consistent with the lacustrine sedimentary environment of the local organic-rich Barremian-Aptian Red and Grey Cuvo formations, as well as previous Re-Os studies showing highly radiogenic initial $^{187}Os/^{188}Os$ for the equivalent pre-salt lacustrine strata of the conjugated Brazilian marginal basins. Thus, Os isotope composition can be used for the source rock tracing of the bitumen in this study. Furthermore, the Os isotope composition of the bitumen also demonstrates hydrothermal fluids which may have had an unradiogenic mantle-like $^{187}Os/^{188}Os$ had little to no influence on the bitumen $^{187}Os/^{188}Os$.

## Figure captions

Figure 1 Location of the Kwanza Basin and the pre-salt reservoir in this study (Google Map; Jerram et al., 2019; Masse and Laurent, 2016). (a) The location of the studied area in Africa. (b) The location of the studied reservoir and the cross-section (A-A') shown in (c), offshore Angola. (c) Seismic cross-section showing the geological structure of the studied reservoir. (d) The stratigraphy of the studied well.

Figure 2 Matrices and macerals of the Chela, Grey and Red Cuvo formations (under reflected light if not specified as polarized and fluorescence). The only organic matter observed in the Chela Formation carbonate is the pore-filling anisotropic bitumen with no fluorescence. The carbonates are crystallized and exhibit a pale yellowish fluorescence. The Grey Cuvo Formation is characterized by rich humic coaly remains in carbonated and argillaceous siltstones. Fluorescent rhombs of the carbonate are observed. The occasionally carbonated siliciclastic rocks of the Red Cuvo Formation contain micro-granular organic matter as thin reflective networks indicating a sapropelic depositional environment, humic coaly remains originated from terrestrial land plants in lower content than the Grey Cuvo Formation, and scarce vuggy bitumen. The absence of fluorescence due to high maturity obstructs better characterization of the organic matter.

Figure 3 Illustration of an ASCI determination process. Each vial is represented in blue with its composition reported on it. All percentages are wt.%. In this illustration, the ASCI is ranked 5 as a solid deposit is observed when *n*-heptane concentration is equal to or more than 25 wt.%.

Figure 4 Organic geochemistry characteristics of the reservoir. (a) The TOC (pentane-insoluble bitumen) contents of the Chela Formation carbonate rocks, (b) the reflectance, and (c) Tmax of bitumen versus depth. See text for discussion.

Figure 5 Model of the charging history of the studied reservoir. The reservoir was firstly charged with crude oil (a) which was then transformed into bitumen by the magmatism-derived hot $CO_2$ through asphaltene progressive precipitation and thermal cracking (b). Mobile hydrocarbons may have also been driven away from the reservoir by the $CO_2$ influx.

Figure 6 Model for the first stage of bitumen formation through the asphaltene precipitation induced by the cooled magmatism-associated $CO_2$. Initially, it was the crude oil that was accumulated in the reservoir. When the magmatism-derived $CO_2$ started to charge into the reservoir from or accumulated at the top of the reservoir, asphaltene precipitation was induced immediately at the contact (①). The continued charge of $CO_2$ resulted in a decreasing concentration gradient with depth within the reservoir inducing the precipitation of progressively less asphaltene from crude oil (②). A higher concentration of $CO_2$ induced the precipitation of more asphaltene in the higher position. Before the thermal cracking, the multiple $CO_2$ influxes may have driven the mobile fractions of crude oil away from the reservoir (③).

Figure 7 The Re and Os concentrations of the whole rock and bitumen versus depth. For the whole rock samples, the overall trend observed is the decrease in Re and Os concentrations with depth as shown in (a) and (b). For the bitumen, the Re concentrations increase with depth between 5300 and 5400 m (c), whereas the Os concentrations generally increase with depth (d).

Figure 8 Bitumen Re-Os isotope plots for the Kwanza Basin: (a) $^{187}Re/^{188}Os$ vs $^{187}Os/^{188}Os$ plot (*IsoplotR*) of all the samples defining a Model 3 age of 174 ± 37 Ma and insert plot shows the deviation of samples from the regression line yielding a 174 Re-Os date; (b) Inverse Re-Os isochron defined by all the samples; (c) $^{187}Re/^{188}Os$ vs $^{187}Os/^{188}Os$ plot of All the samples excluding the PRA9 and 10 defining a Model 1 age of 131 ± 21 Ma and insert plot shows the deviation of samples from the regression line yielding a 131 Re-Os date; (d) Inverse Re-Os isochron defined by all the sample excluding the PRA9 and 10; (e) a Model 1 Re-Os isochron defined by the PRA2, 3, 5, 6, and 8 samples yielding an age of 116 ± 29 Ma which is the best estimate of the bitumen formation timing. See text for discussion.

## Table captions

Table 1 The TOC (bitumen) contents, Tmax and $BR_o$ of the Chela Formation samples.

Table 2 The composition and solubility of the Chela Formation bitumen.

Table 3 The Re-Os data synopsis of the Chela Formation samples and the $Os_i$ at critical timings of the studied petroleum system.

## References


Behar, F., Beaumont, V., De B. Penteado, H.L., 2001. Rock-Eval 6 Technology: Performances and Developments. Oil & Gas Science and Technology 56, 111-134.

Behar, F., Ungerer, P., Kressmann, S., Rudkiewicz, J., 1991. Thermal evolution of crude oils in sedimentary basins: experimental simulation in a confined system and kinetic modeling. Oil & Gas Science and Technology 46, 151-181.

Brownfield, M.E., Charpentier, R.R., 2006. Geology and total petroleum systems of the West-Central Coastal province (7203), West Africa, Bulletin, Version 1.0 ed, p. 59.

Burwood, R., 1999. Angola: source rock control for Lower Congo Coastal and Kwanza Basin petroleum systems. Geological Society, London, Special Publications 153, 181-194.

Ceraldi, T.S., Green, D., 2017. Evolution of the South Atlantic lacustrine deposits in response to Early Cretaceous rifting, subsidence and lake hydrology. Geological Society, London, Special Publications 438, 77-98.

Cohen, K.M., Finney, S.C., Gibbard, P.L., Fan, J.-X., 2013. The ICS international chronostratigraphic chart. Episodes 36, 199-204.

Comin-Chiaramonti, P., De Min, A., Girardi, V.A.V., Ruberti, E., 2011. Post-Paleozoic magmatism in Angola and Namibia: A review, Volcanism and Evolution of the African Lithosphere, pp. 223-247.

Corrick, A.J., Hall, P.A., Gong, S., McKirdy, D.M., Selby, D., Trefry, C., Ross, A.S., 2020. A second type of highly asphaltic crude oil seepage stranded on the South Australian coastline. Marine and Petroleum Geology 112, 104062.

Corrick, A.J., Selby, D., McKirdy, D.M., Hall, P.A., Gong, S., Trefry, C., Ross, A.S., 2019. Remotely constraining the temporal evolution of offshore oil systems. Sci Rep 9, 1327.

Coward, M.P., Purdy, E.G., Ries, A.C., Smith, D.G., 1999. The distribution of petroleum reserves in basins of the South Atlantic margins. Geological Society, London, Special Publications 153, 101-131.

Creaser, R., Szatmari, P., Milani, E., 2008. Extending Re–Os shale geochronology to lacustrine depositional systems: a case study from the major hydrocarbon source rocks of the Brazilian Mesozoic marginal basins, Proceedings of the 33rd International Geological Congress, Oslo.

Cumming, V.M., Selby, D., Lillis, P.G., 2012. Re–Os geochronology of the lacustrine Green River Formation: Insights into direct depositional dating of

773 lacustrine successions, Re–Os systematics and paleocontinental weathering.
774 Earth and Planetary Science Letters 359-360, 194-205.

775 Cumming, V.M., Selby, D., Lillis, P.G., Lewan, M.D., 2014. Re–Os geochronology
776 and Os isotope fingerprinting of petroleum sourced from a Type I lacustrine
777 kerogen: Insights from the natural Green River petroleum system in the Uinta
778 Basin and hydrous pyrolysis experiments. Geochimica et Cosmochimica Acta
779 138, 32-56.

780 Curiale, J.A., 2008. Oil–source rock correlations – Limitations and recommendations.
781 Organic Geochemistry 39, 1150-1161.

782 Danforth, A., 1998. Petroleum systems of the coastal Kwanza and Benguela basins,
783 Angola. Houston Geological Society Bulletin 41, 18,19, 21.

784 Davies, J.H.F.L., Sheldrake, T.E., Reimink, J.R., Wotzlaw, J.-F., Moeck, C., Finlay,
785 A., 2018. Investigating Complex Isochron Data Using Mixture Models.
786 Geochemistry, Geophysics, Geosystems 19, 4035-4047.

787 Denis, M., Kluska, J.-M., 2017. South Kwanza Basin (Offshore Angola) as a Major
788 Cornerstone of West African Margin, AAPG Annual Convention and
789 Exhibition, Houston, Texas.

790 DiMarzio, J.M., Georgiev, S.V., Stein, H.J., Hannah, J.L., 2018. Residency of
791 rhenium and osmium in a heavy crude oil. Geochimica et Cosmochimica Acta
792 220, 180-200.

793 Ehrenbrink, B.P., Ravizza, G., 1996. Continental runoff of osmium into the Baltic
794 Sea. Geology 24, 327-330.

795 Evenick, J.C., 2021. Examining the relationship between Tmax and vitrinite
796 reflectance: An empirical comparison between thermal maturity indicators.
797 Journal of Natural Gas Science and Engineering 91, 103946.

798 Faure, G., 1986. Principles of isotope geology, 2 ed. John Weily & Sons, New York.

799 Finlay, A.J., Selby, D., Osborne, M.J., 2011. Re-Os geochronology and
800 fingerprinting of United Kingdom Atlantic margin oil: Temporal implications
801 for regional petroleum systems. Geology 39, 475-478.

802 Finlay, A.J., Selby, D., Osborne, M.J., 2012. Petroleum source rock identification of
803 United Kingdom Atlantic Margin oil fields and the Western Canadian Oil
804 Sands using Platinum, Palladium, Osmium and Rhenium: Implications for
805 global petroleum systems. Earth and Planetary Science Letters 313-314,
806 95-104.

807 Finlay, A.J., Selby, D., Osborne, M.J., Finucane, D., 2010. Fault-charged
808 mantle-fluid contamination of United Kingdom North Sea oils: Insights from
809 Re-Os isotopes. Geology 38, 979-982.

Foulger, G.R., 2018. Origin of the South Atlantic igneous province. Journal of Volcanology and Geothermal Research 355, 2-20.

Gamboa, L., Ferraz, A., Baptista, R., Neto, E.V.S., 2019. Geotectonic Controls on CO2 Formation and Distribution Processes in the Brazilian Pre-Salt Basins. Geosciences 9, 252.

Ge, X., Selby, D., Liu, J., Chen, Y., Cheng, G., Shen, C., 2021. Genetic relationship between hydrocarbon system evolution and Carlin-type gold mineralization: Insights from ReOs pyrobitumen and pyrite geochronology in the Nanpanjiang Basin, South China. Chemical Geology 559, 119953.

Ge, X., Shen, C., Selby, D., Feely, M., Zhu, G., 2020. Petroleum evolution within the Tarim Basin, northwestern China: Insights from organic geochemistry, fluid inclusions, and Re-Os geochronology of the Halahatang oilfield. AAPG Bulletin, 329-355.

Ge, X., Shen, C., Selby, D., Wang, J., Ma, L., Ruan, X., Hu, S., Mei, L., 2018a. Petroleum-generation timing and source in the northern Longmen Shan thrust belt, Southwest China: Implications for multiple oil-generation episodes and sources. AAPG Bulletin 102, 913-938.

Ge, X., Shen, C.b., Selby, D., Deng, D.f., Mei, L.f., 2016. Apatite fission-track and Re-Os geochronology of the Xuefeng uplift, China: Temporal implications for dry gas associated hydrocarbon systems. Geology 44, 491-494.

Ge, X., Shen, C.b., Selby, D., Wang, G.z., Yang, Z., Gong, Y.j., Xiong, S.f., 2018b. Neoproterozoic–Cambrian petroleum system evolution of the Micang Shan uplift, northern Sichuan Basin, China: Insights from pyrobitumen rhenium–osmium geochronology and apatite fission-track analysis. AAPG Bulletin 102, 1429-1453.

Georgiev, S.V., Stein, H.J., Hannah, J.L., Galimberti, R., Nali, M., Yang, G., Zimmerman, A., 2016. Re-Os dating of maltenes and asphaltenes within single samples of crude oil. Geochimica et Cosmochimica Acta 179, 53-75.

Georgiev, S.V., Stein, H.J., Hannah, J.L., Yang, G., Markey, R.J., Dons, C.E., Pedersen, J.H., di Primio, R., 2019. Comprehensive evolution of a petroleum system in absolute time: The example of Brynhild, Norwegian North Sea. Chemical Geology 522, 260-282.

Girard, J.-P., Miguel, G., 2017. Evidence of high temperature hydrothermal regimes in the Presalt series, Kwanza basin, Offshore Angola, AAPG Annual Convention and Exhibition, Houston, Texas.

Girard, J.-P., Miguel, G.S., 2018. Hydrothermal Diagenesis and Reservoir Quality in the Pre-Salt Carbonate-Clastic Series of the Kwanza Basin, Offshore Angola, AAPG ACE.

Girard, J.P., Miguel, G.S., Godeau, N., 2017. Pervasive hydrothermal diagenesis in the Pre-salt carbonate reservoirs of the Kwanza basin, offshore Angola, IMS 2017.

Gonzalez, D.L., Vargas, F.M., Hirasaki, G.J., Chapman, W.G., 2008. Modeling Study of CO2-Induced Asphaltene Precipitation. Energy & Fuels 22, 757-762.

Hu, W., Jin, Z., Song, Y., Sun, R., Duan, Z., 2004. Theoretical Calculation Model of Heat Transfer for Deep‐derived Supercritical Fluids with a Case Study. Acta Geologica Sinica‐English Edition 78, 221-229.

Huang, S., Qin, M., Selby, D., Liu, Y., Xu, Q., He, Z., Liu, Z., Liu, J., 2018. Geochemistry characteristics and Re-Os isotopic dating of Jurassic oil sands in the northwestern margin of the Junggar Basin. Earth Science Frontiers 25, 254-266.

Hurtig, N.C., Georgiev, S.V., Stein, H.J., Hannah, J.L., 2019. Re-Os systematics in petroleum during water-oil interaction: The effects of oil chemistry. Geochimica et Cosmochimica Acta 247, 142-161.

Hurtig, N.C., Georgiev, S.V., Zimmerman, A., Yang, G., Goswami, V., Hannah, J.L., Stein, H.J., 2020. Re-Os geochronology for the NIST RM 8505 crude oil: The importance of analytical protocol and uncertainty. Chemical Geology 539, 119381.

Hwang, R.J., Teerman, S.C., Carlson, R.M., 1998. Geochemical comparison of reservoir solid bitumens with diverse origins. Organic Geochemistry 29, 505-517.

Ishmael, M.P.E., Lukawski, M.Z., Tester, J.W., 2016. Isobaric heat capacity (Cp) measurements of supercritical fluids using flow calorimetry: equipment design and experimental validation with carbon dioxide, methanol, and carbon dioxide-methanol mixtures. The Journal of Supercritical Fluids 117, 72-79.

Jacob, H., 1989. Classification, structure, genesis and practical importance of natural solid oil bitumen ("migrabitumen"). International Journal of Coal Geology 11, 65-79.

Jerram, D.A., Sharp, I.R., Torsvik, T.H., Poulsen, R., Watton, T., Freitag, U., Halton, A., Sherlock, S.C., Malley, J.A.S., Finley, A., Roberge, J., Swart, R., Puigdefabregas, C., Ferreira, C.H., Machado, V., 2019. Volcanic constraints on the unzipping of Africa from South America: Insights from new geochronological controls along the Angola margin. Tectonophysics 760, 252-266.

Karner, G.D., Gambôa, L.A.P., 2007. Timing and origin of the South Atlantic pre-salt sag basins and their capping evaporites. Geological Society, London, Special Publications 285, 15-35.

886 Katz, B.J., Lin, F., 2021. Consideration of the limitations of thermal maturity with
887 respect to vitrinite reflectance, Tmax, and other proxies. AAPG Bulletin 105,
888 695-720.

889 Kendall, B.S., Creaser, R.A., Ross, G.M., Selby, D., 2004. Constraints on the timing
890 of Marinoan “Snowball Earth” glaciation by 187Re–187Os dating of a
891 Neoproterozoic, post-glacial black shale in Western Canada. Earth and
892 Planetary Science Letters 222, 729-740.

893 Kohn, B.P., Green, P.F., 2002. Low temperature thermochronology: from tectonics
894 to landscape evolution. Tectonophysics 349, 1-4.

895 Lafargue, E., Marquis, F., Pillot, D., 1998. Rock-Eval 6 Applications in
896 Hydrocarbon Exploration, Production, and Soil Contamination Studies. Revue
897 de l'institut français du pétrole 53, 421-437.

898 Lei, R., Xiong, Y., Li, Y., Zhang, L., 2018. Main factors influencing the formation of
899 thermogenic solid bitumen. Organic Geochemistry 121, 155-160.

900 Li, Y., Vermeesch, P., 2021. Inverse isochron regression for Re–Os, K–Ca and other
901 chronometers. Geochronology Discussions, 1-8.

902 Lillis, P.G., Selby, D., 2013. Evaluation of the rhenium–osmium geochronometer in
903 the Phosphoria petroleum system, Bighorn Basin of Wyoming and Montana,
904 USA. Geochimica et Cosmochimica Acta 118, 312-330.

905 Liu, J.j., Selby, D., 2018. A matrix-matched reference material for validating
906 petroleum Re-Os measurements. Geostandards and Geoanalytical Research 42,
907 97-113.

908 Liu, J.J., Selby, D., Obermajer, M., Mort, A., 2018. Rhenium–osmium
909 geochronology and oil–source correlation of the Duvernay petroleum system,
910 Western Canada sedimentary basin: Implications for the application of the
911 rhenium–osmium geochronometer to petroleum systems. AAPG Bulletin 102,
912 1627-1657.

913 Liu, J.j., Selby, D., Zhou, H., Pujol, M., 2019. Further evaluation of the Re-Os
914 systematics of crude oil: Implications for Re-Os geochronology of petroleum
915 systems. Chemical Geology 513, 1-22.

916 Loma, R., Tritlla, J., Cerdà, M., Sanders, C., Carrasco, A., Herrá, A., Gerona, M.,
917 Mañas, M., Boix, C., 2018. Hydrothermal Flushing and Calcite Precipitation as
918 Main Modifiers of a Pre-Salt Reservoir in Kwanza Basin (Angola).

919 Lúcio, T., Souza Neto, J.A., Selby, D., 2020. Late Barremian / Early Aptian Re–Os
920 age of the Ipubi Formation black shales: Stratigraphic and paleoenvironmental
921 implications for Araripe Basin, northeastern Brazil. Journal of South American
922 Earth Sciences 102, 102699.

923 Mahdaoui, F., Michels, R., Reisberg, L., Pujol, M., Poirier, Y., 2015. Behavior of Re
924 and Os during contact between an aqueous solution and oil: Consequences for
925 the application of the Re–Os geochronometer to petroleum. Geochimica et
926 Cosmochimica Acta 158, 1-21.

927 Mahdaoui, F., Reisberg, L., Michels, R., Hautevelle, Y., Poirier, Y., Girard, J.-P.,
928 2013. Effect of the progressive precipitation of petroleum asphaltenes on the
929 Re–Os radioisotope system. Chemical Geology 358, 90-100.

930 Marsh, J.S., Swart, R., 2018. The Bero Volcanic Complex: Extension of the
931 Paraná-Etendeka Igneous Province into SW Angola. Journal of Volcanology
932 and Geothermal Research 355, 21-31.

933 Marzoli, A., Melluso, L., Morra, V., Renne, P.R., Sgrosso, I., D'Antonio, M., Duarte
934 Morais, L., Morais, E.A.A., Ricci, G., 1999. Geochronology and petrology of
935 Cretaceous basaltic magmatism in the Kwanza basin (western Angola), and
936 relationships with the Paranà-Etendeka continental flood basalt province.
937 Journal of Geodynamics 28, 341-356.

938 Masse, P., Laurent, O., 2016. Geological exploration of Angola from Sumbe to
939 Namibe: A review at the frontier between geology, natural resources and the
940 history of geology. Comptes Rendus Geoscience 348, 80-88.

941 Meisel, T., Walker, R.J., Irving, A.J., Lorand, J.-P., 2001. Osmium isotopic
942 compositions of mantle xenoliths: a global perspective. Geochimica et
943 Cosmochimica Acta 65, 1311-1323.

944 Melankholina, E.N., Sushchevskaya, N.M., 2018. Tectono-magmatic evolution of
945 the South Atlantic continental margins with respect to opening of the ocean.
946 Geotectonics 52, 173-193.

947 Meyer, R.F., De Witt, W., 1990. Definition and world resources of natural bitumens.
948 United States Department of the Interior, United States Geological Survey.

949 Miguel, G.S., Teboul, P.A., Virgone, A., Barbat, L., Girard, J.-P., Kenter, J., 2017. A
950 Review of Carbonate Continental Systems in Active Rift Settings (Offshore
951 Angola)–A Combined Subsurface and Outcrop Study for Derisking Reservoir
952 Presence, AAPG Annual Convention and Exhibition.

953 Monger, T., Fu, J., 1987. The nature of CO2-induced organic deposition, SPE
954 Annual Technical Conference and Exhibition. Society of Petroleum Engineers.

955 Nali, M., Caccialanza, G., Ghiselli, C., Chiaramonte, M.A., 2000. Tmax of
956 asphaltenes: a parameter for oil maturity assessment. Organic Geochemistry 31,
957 1325-1332.

958 Nalwaya, V., Tantayakom, V., Piumsomboon, P., Fogler, S., 1999. Studies on
959 Asphaltenes through Analysis of Polar Fractions. Industrial & Engineering
960 Chemistry Research 38, 964-972.

961 Pasley, M., Wilson, E., Abreu, V., Brandao, M., Telles, A., 1998. Lower Cretaceous
962 stratigraphy and source rock distribution in pre-salt basins of the South
963 Atlantic: Comparison of Angola and southern Brazil. American Association of
964 Petroleum Geologists Bulletin 82, 1949.

965 Passade-Boupat, N., Zhou, H., Rondon-Gonzalez, M., 2013. Asphaltene
966 Precipitation From Crude Oils: How To Predict It And To Anticipate
967 Treatment?, SPE Middle East Oil and Gas Show and Conference. Society of
968 Petroleum Engineers.

969 Pietras, J.T., Selby, D., Brembs, R., Dennett, A., 2020. Tracking drainage basin
970 evolution, continental tectonics, and climate change: Implications from
971 osmium isotopes of lacustrine systems. Palaeogeography, Palaeoclimatology,
972 Palaeoecology 537, 109471.

973 Poirier, A., Hillaire-Marcel, C., 2011. Improved Os-isotope stratigraphy of the Arctic
974 Ocean. Geophysical Research Letters 38.

975 Quirk, D.G., Hertle, M., Jeppesen, J.W., Raven, M., Mohriak, W.U., Kann, D.J.,
976 Nørgaard, M., Howe, M.J., Hsu, D., Coffey, B., Mendes, M.P., 2013. Rifting,
977 subsidence and continental break-up above a mantle plume in the central South
978 Atlantic. Geological Society, London, Special Publications 369, 185-214.

979 Quirk, D.G., Schødt, N., Lassen, B., Ings, S.J., Hsu, D., Hirsch, K.K., Von Nicolai,
980 C., 2012. Salt tectonics on passive margins: examples from Santos, Campos
981 and Kwanza basins. Geological Society, London, Special Publications 363,
982 207-244.

983 Rahman, M.W., Rimmer, S.M., 2014. Effects of rapid thermal alteration on coal:
984 Geochemical and petrographic signatures in the Springfield (No. 5) Coal,
985 Illinois Basin. International Journal of Coal Geology 131, 214-226.

986 Rahman, M.W., Rimmer, S.M., Rowe, H.D., 2018. The impact of rapid heating by
987 intrusion on the geochemistry and petrography of coals and organic-rich shales
988 in the Illinois Basin. International Journal of Coal Geology 187, 45-53.

989 Rahman, M.W., Rimmer, S.M., Rowe, H.D., Huggett, W.W., 2017a. Carbon isotope
990 analysis of whole-coal and vitrinite from intruded coals from the Illinois Basin:
991 No isotopic evidence for thermogenic methane generation. Chemical Geology
992 453, 1-11.

993 Rahman, M.W., Veach, D., Jayakumar, R., Esmaili, S., 2017b. Application of
994 Organic Geochemistry on Assessment of Fluid Behavior and Oil Migration
995 within the Woodford Shale in the Anadarko Basin, Unconventional Resources
996 Technology Conference, Austin, Texas.

997 Rogers, M., McAlary, J., Bailey, N., 1974. Significance of reservoir bitumens to
998 thermal-maturation studies, Western Canada Basin. AAPG Bulletin 58,
999 1806-1824.

Rooney, A.D., Chew, D.M., Selby, D., 2011. Re–Os geochronology of the Neoproterozoic–Cambrian Dalradian Supergroup of Scotland and Ireland: Implications for Neoproterozoic stratigraphy, glaciations and Re–Os systematics. Precambrian Research 185, 202-214.

Rooney, A.D., Selby, D., Lewan, M.D., Lillis, P.G., Houzay, J.-P., 2012. Evaluating Re–Os systematics in organic-rich sedimentary rocks in response to petroleum generation using hydrous pyrolysis experiments. Geochimica et Cosmochimica Acta 77, 275-291.

Sai, Y.m., Jin, K.y., Luo, M.z., Tian, H., Li, J., Liu, J.j., 2020. Recent progress on the research of Re–Os geochronology and Re–Os elemental and isotopic systematics in petroleum systems. Journal of Natural Gas Geoscience 5, 355-365.

Saller, A., Rushton, S., Buambua, L., Inman, K., McNeil, R., Dickson, J.A.D., 2016. Presalt stratigraphy and depositional systems in the Kwanza Basin, offshore Angola. AAPG Bulletin 100, 1135-1164.

Scarlett, A.G., Holman, A.I., Georgiev, S.V., Stein, H.J., Summons, R.E., Grice, K., 2019. Multi-spectroscopic and elemental characterization of southern Australian asphaltites. Organic Geochemistry 133, 77-91.

Schoellkopf, N.B., Patterson, B.A., 2000. AAPG Memoir 73, Chapter 25: Petroleum Systems of Offshore Cabinda, Angola.

Selby, D., Creaser, R., Dewing, K., Fowler, M., 2005. Evaluation of bitumen as a Re–Os geochronometer for hydrocarbon maturation and migration: A test case from the Polaris MVT deposit, Canada. Earth and Planetary Science Letters 235, 1-15.

Selby, D., Creaser, R.A., 2003. Re–Os geochronology of organic rich sediments: an evaluation of organic matter analysis methods. Chemical Geology 200, 225-240.

Selby, D., Creaser, R.A., 2005. Direct radiometric dating of hydrocarbon deposits using rhenium-osmium isotopes. Science 308, 1293-1295.

Selby, D., Creaser, R.A., Fowler, M.G., 2007a. Re–Os elemental and isotopic systematics in crude oils. Geochimica et Cosmochimica Acta 71, 378-386.

Selby, D., Creaser, R.A., Stein, H.J., Markey, R.J., Hannah, J.L., 2007b. Assessment of the 187Re decay constant by cross calibration of Re–Os molybdenite and U–Pb zircon chronometers in magmatic ore systems. Geochimica et Cosmochimica Acta 71, 1999-2013.

Serié, C., Huuse, M., Schødt, N.H., Brooks, J.M., Williams, A., 2017. Subsurface fluid flow in the deep-water Kwanza Basin, offshore Angola. Basin Research 29, 149-179.

Shi, C., Cao, J., Bao, J., Zhu, C., Jiang, X., Wu, M., 2015. Source characterization of highly mature pyrobitumens using trace and rare earth element geochemistry: Sinian–Paleozoic paleo-oil reservoirs in South China. Organic Geochemistry 83-84, 77-93.

Shi, C., Jian, C., Hu, W., Selby, D., Hong, L., 2016. Hydrocarbon-source correlation and timing under post-mature conditions using Re-Os geochronology: The Neoproterozoic Dengying formation of the Sichuan basin, southwestern China, International Conference and Exhibition, Barcelona, Spain, 3-6 April 2016.

Smoliar, M.I., Walker, R.J., Morgan, J.W., 1996. Re-Os ages of group IIA, IIIA, IVA, and IVB iron meteorites. Science 271, 1099-1102.

Srivastava, R.K., Huang, S.S., Dong, M., 1999. Asphaltene Deposition During CO2 Flooding. SPE-59092-PA 14, 235-245.

Stein, H.J., Hannah, J.L., 2016. A gallery of oil components, their metals and Re-Os signatures, EGU General Assembly Conference Abstracts.

Su, A., Chen, H.h., Feng, Y.x., Zhao, J.x., Nguyen, A.D., Wang, Z.c., Long, X.p., 2020. Dating and characterizing primary gas accumulation in Precambrian dolomite reservoirs, Central Sichuan Basin, China: Insights from pyrobitumen Re-Os and dolomite U-Pb geochronology. Precambrian Research 350, 105897.

Szatmari, P., Milani, E.J., 2016. Tectonic control of the oil-rich large igneous-carbonate-salt province of the South Atlantic rift. Marine and Petroleum Geology 77, 567-596.

Teboul, P.-A., Durlet, C., Girard, J.-P., Dubois, L., San Miguel, G., Virgone, A., Gaucher, E.C., Camoin, G., 2019. Diversity and origin of quartz cements in continental carbonates: Example from the Lower Cretaceous rift deposits of the South Atlantic margin. Applied Geochemistry 100, 22-41.

Teboul, P.-A., Kluska, J.-M., Marty, N.C.M., Debure, M., Durlet, C., Virgone, A., Gaucher, E.C., 2017. Volcanic rock alterations of the Kwanza Basin, offshore Angola - Insights from an integrated petrological, geochemical and numerical approach. Marine and Petroleum Geology 80, 394-411.

Torsvik, T.H., Rousse, S., Labails, C., Smethurst, M.A., 2009. A new scheme for the opening of the South Atlantic Ocean and the dissection of an Aptian salt basin. Geophysical Journal International 177, 1315-1333.

Tritlla, J., Esteban, M., Loma, R., Mattos, A., Sanders, C., Luca, P.H.V.D., Carrasco, A., Gerona, M., Herrá, A., Carballo, J., 2019. Where have most of the carbonates gone? Silicified Aptian pre-salt microbial (?) carbonates in South Atlantic basins (Brazil and Angola), 16th International Meeting of Carbonate Sedimentologists, Palma de Mallorca, Spain, pp. 9-11.

Tritlla, J., Loma, R., Cerdà, M., Sanders, C., Sanchez Perez-Cejuela, V., Benito, V., Carrasco, A., Peña, L., Herrá, A., Gerona, M., Levresse, G., Upstream, R.,

Exploracion, Madrid, Madrid, S., Grup, S., Caimari, Mallorca, S., 2018. Pre-Salt Lacustrine Carbonates, Diagenetic Silicification and Hydrothermal Overprinting in Kwanza Basin (Offshore Angola): A Tale of Two Silicas.

Uncini, G., Brandão, M., Giovannelli, A., 1998. Neocomian-Upper Aptian Pre-Salt sequence of southern Kwanza Basin: a regional view, ABGP/AAPG International Conference and Exhibition November 8-11, 1998, Rio de Janeiro, Brazil.

Vermeesch, P., 2018. IsoplotR: A free and open toolbox for geochronology. Geoscience Frontiers 9, 1479-1493.

Wang, J., Tenger, Liu, W., Ma, L., Tao, C., Wang, P., 2019. Definition of Petroleum Generating Time for Lower Cambrian Bitumen of the Kuangshanliang in the West Sichuan Basin, China: Evidence from Re-Os Isotopic Isochron Age. 2019, 1-2.

Wang, P.P., Hu, Y.Z., Liu, L., Jiang, X.J., Li, C., Bartholomew, C.J., Zhang, G.Q., 2017. Re-Os Dating of Bitumen from Paleo-Oil Reservoir in the Qinglong Antimony Deposit, Guizhou Province, China and Its Geological Significance. Acta Geologica Sinica (English Edition) 91, 2153-2163.

White, N., Thompson, M., Barwise, T., 2003. Understanding the thermal evolution of deep-water continental margins. Nature 426, 334-343.

Wu, Z., Peng, P., Fu, J., Sheng, G., Liu, D., 2000. Bitumen associated with petroleum formation, evolution and alteration-review and case studies in China. Developments in petroleum science, 401-443.

Xu, W., Ruhl, M., Jenkyns, Hugh C., Hesselbo, Stephen P., Riding, James B., Selby, D., Naafs, B.David A., Weijers, Johan W.H., Pancost, Richard D., Tegelaar, Erik W., Idiz, Erdem F., 2017. Carbon sequestration in an expanded lake system during the Toarcian oceanic anoxic event. Nature Geoscience 10, 129-134.

Yang, S., Horsfield, B., 2020. Critical review of the uncertainty of Tmax in revealing the thermal maturity of organic matter in sedimentary rocks. International Journal of Coal Geology 225, 103500.

Zanganeh, P., Dashti, H., Ayatollahi, S., 2018. Comparing the effects of CH4, CO2, and N2 injection on asphaltene precipitation and deposition at reservoir condition: a visual and modeling study. Fuel 217, 633-641.

Zhou, H.g., Passade-Boupat, N., Rondon Gonzalez, M., 2012. Workflow for asphaltene precipitation assessment and mitigation strategies, Abu Dhabi International Petroleum Conference and Exhibition. Society of Petroleum Engineers.

Figure 1. Location of the Kwanza Basin and the pre-salt reservoir in this study (Google Map; Jerram et al., 2019; Masse and Laurent, 2016). (a) The location of the studied area in Africa. (b) The location of the studied reservoir and the cross-section (A-A') shown in (c), offshore Angola. (c) Seismic cross-section showing the geological structure of the studied reservoir. (d) The stratigraphy of the studied well.

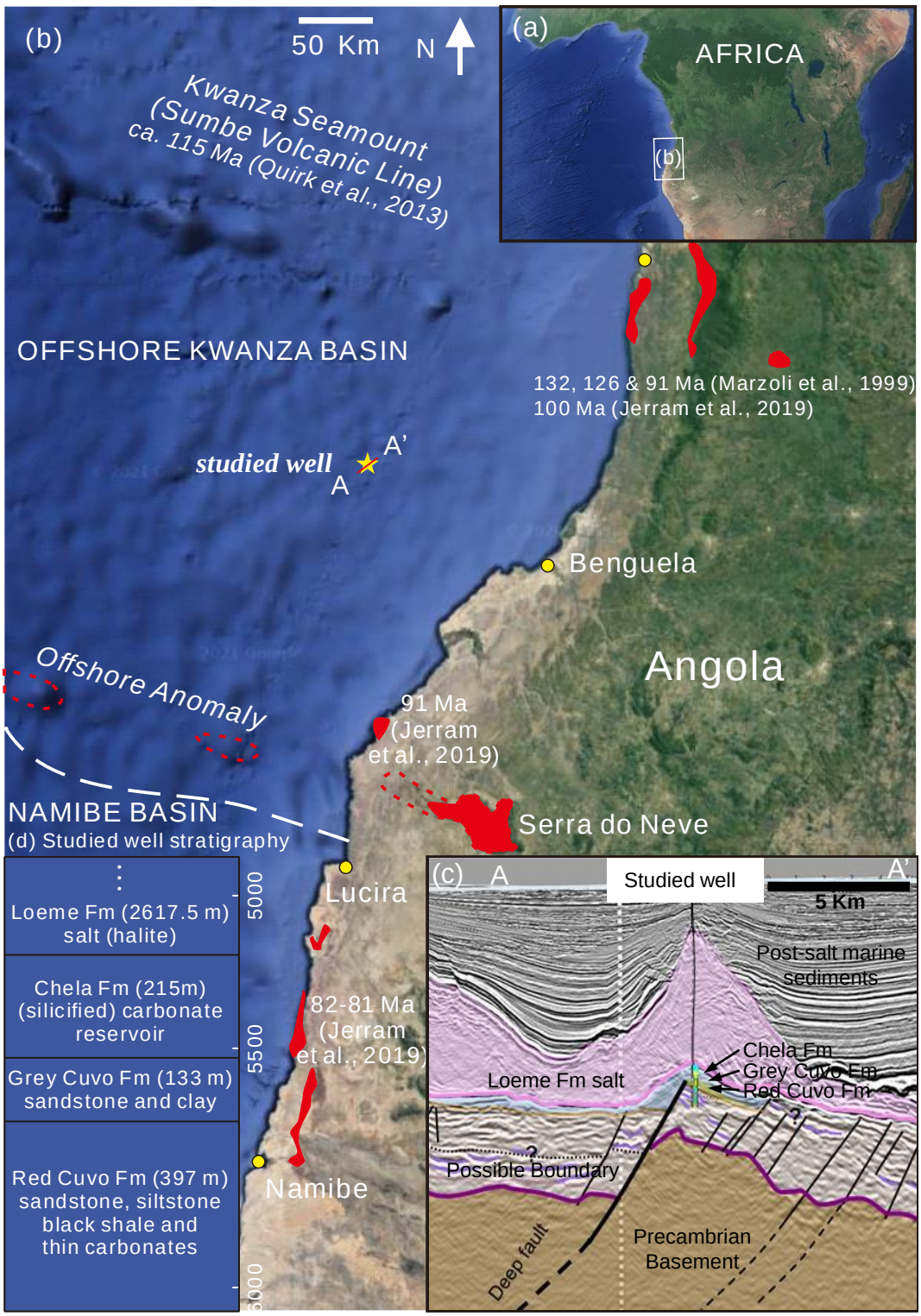

Figure 2. Matrices and macerals of the Chela, Grey and Red Cuvo formations (under reflected light if not specified as polarized and fluorescence). The only organic matter observed in the Chela Formation carbonate is the pore-filling anisotropic bitumen with no fluorescence. The carbonates are crystallized and exhibit a pale yellowish fluorescence. The Grey Cuvo Formation is characterized with rich humic coaly remains in carbonated and argillaceous siltstones. Fluorescent rhombs of the carbonate are observed. The occasionally carbonated siliciclastic rocks of the Red Cuvo Formation contain micro-granular organic matter as thin reflective networks indicating a sapropelic depositional environment, humic coaly remains originated from terrestrial land plant in lower content than the Grey Cuvo Formation, and scarce vuggy bitumen. The absence of fluorescence due to high maturity obstructs better characterization of the organic matter.

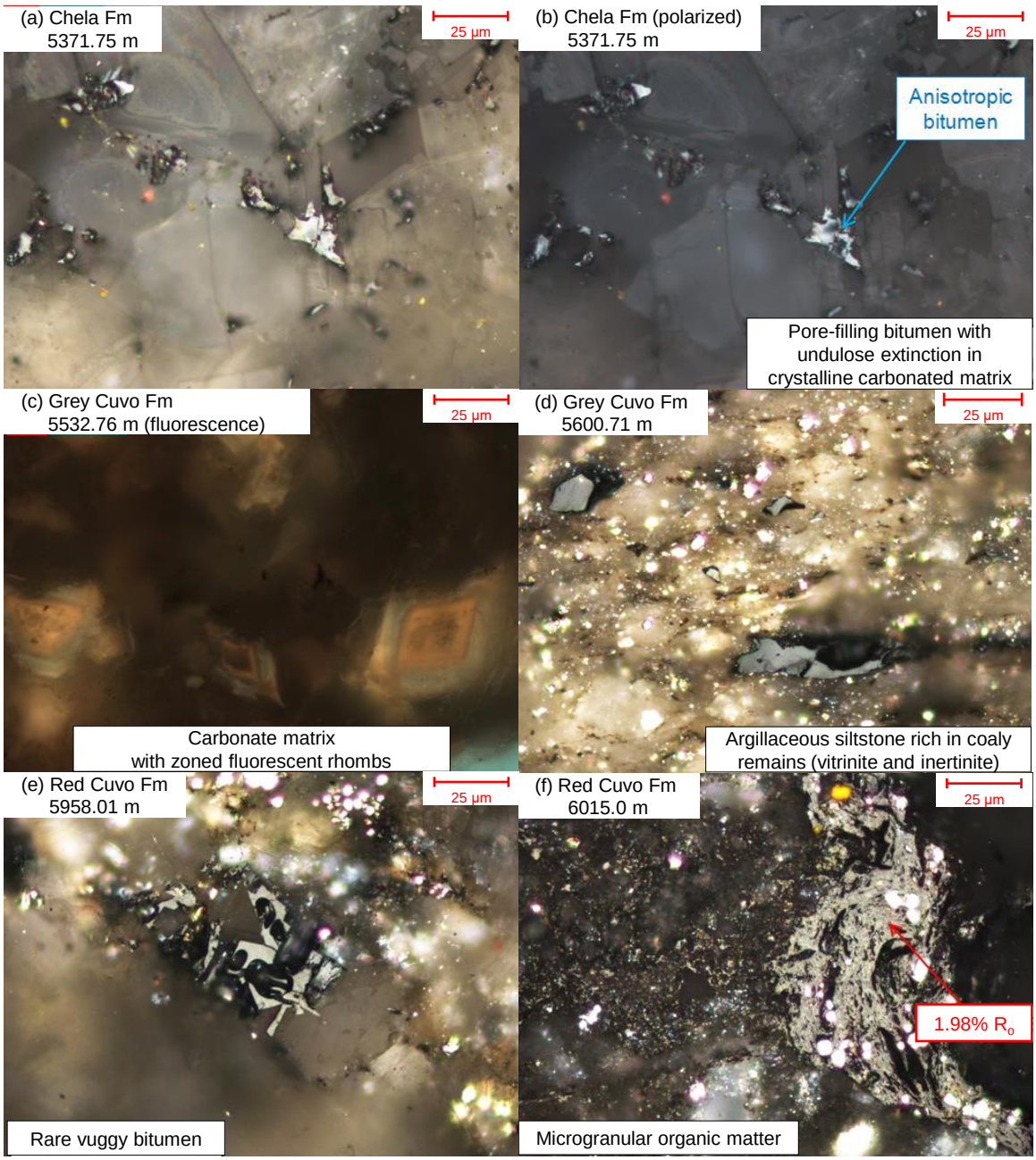

Figure 3. Illustration of an ASCI determination process. Each vial is represented in blue with its composition reported on it. All percentages are wt.%. In this illustration, the ASCI is ranked 5 as a solid deposit is observed when n-heptane concentration is equal to or more than 25 wt.%.

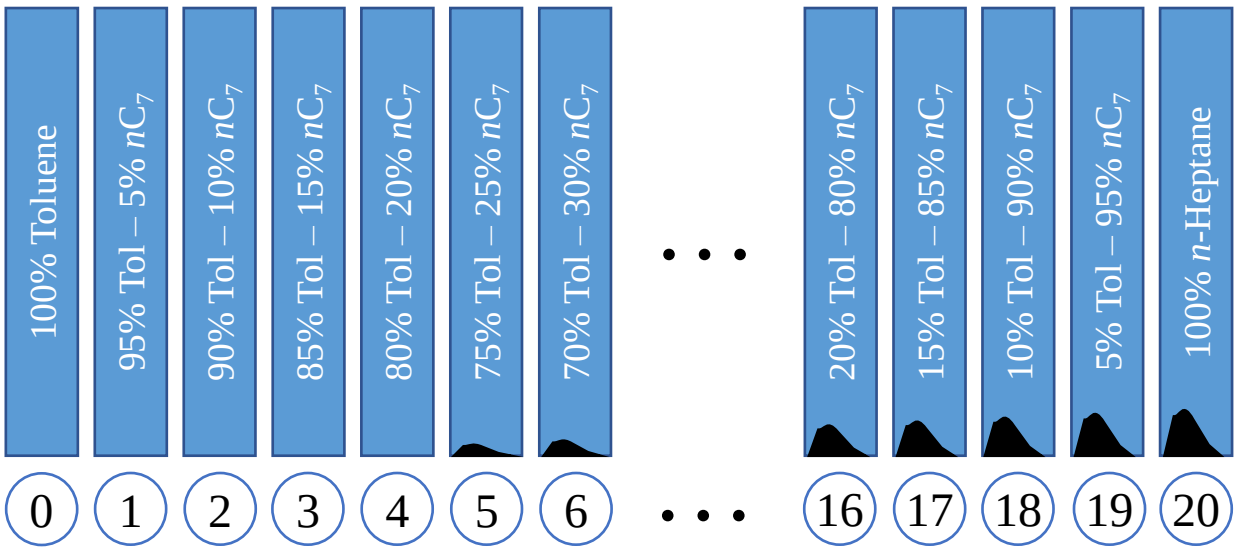

Figure 4. Organic geochemistry characteristics of the reservoir. (a) The TOC (pentane-insoluble bitumen**)** contents of the Chela Formation carbonate rocks, (b) the reflectance, and (c) Tmax of bitumen versus depth. See text for discussion.

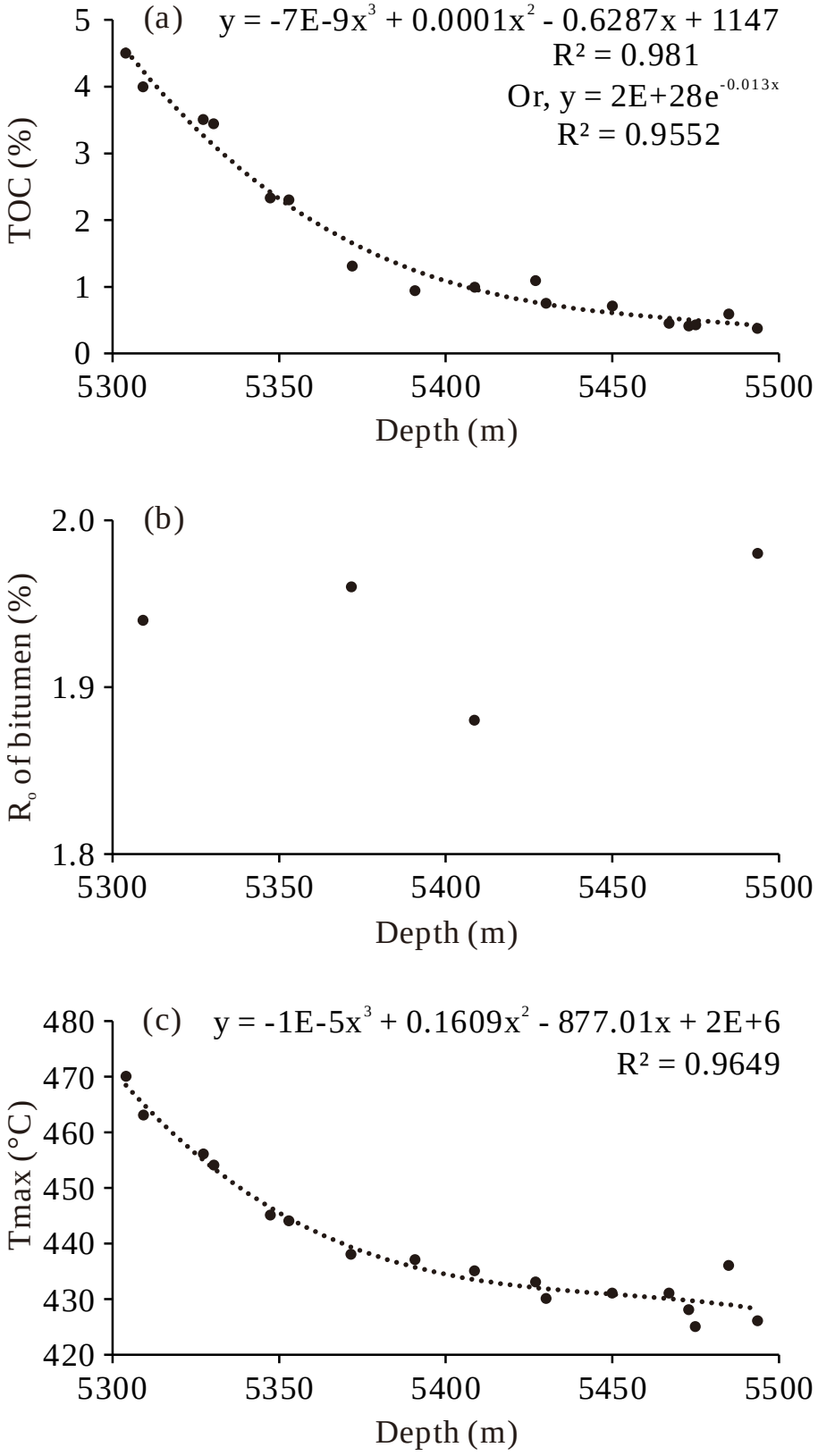

Figure 5. Model of the charging history of the studied reservoir. The reservoir was firstly charged with crude oil (a) which was then transformed into bitumen by the magmatism-derived hot $CO_2$ through asphaltene progressive precipitation and thermal cracking (b). Mobile hydrocarbons may have also been driven away from the reservoir by the $CO_2$ influx.

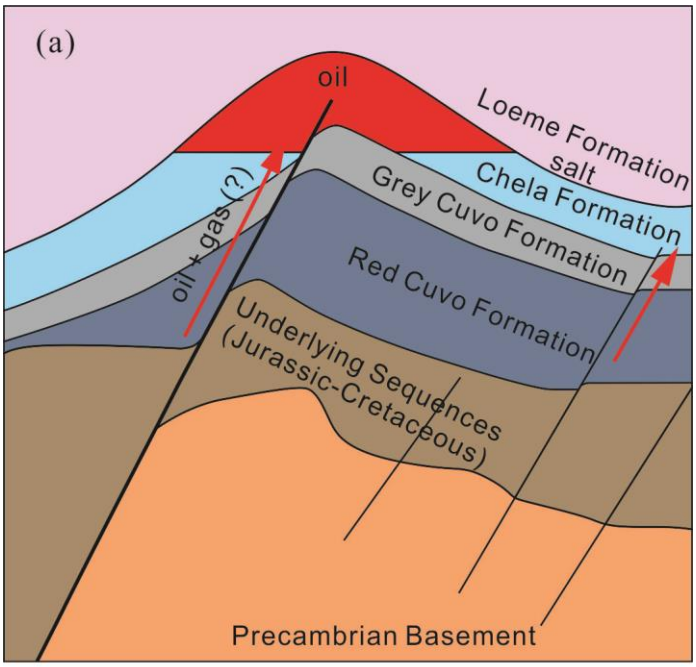


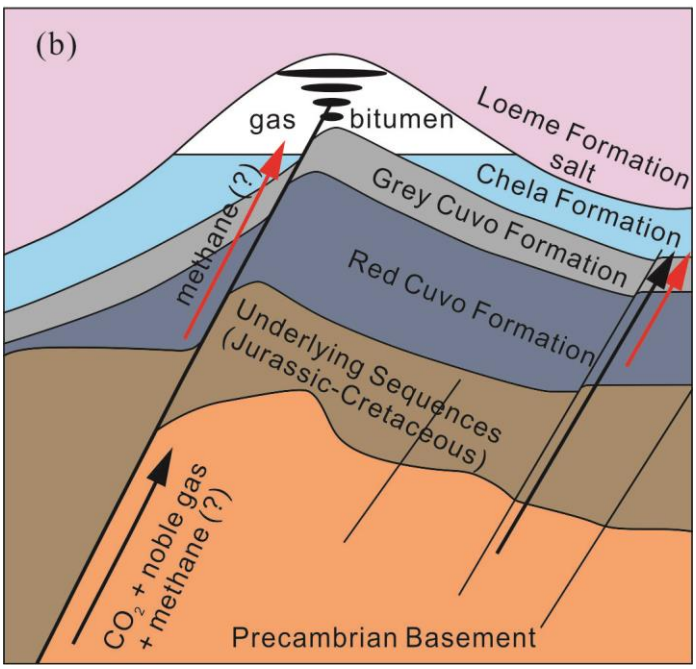

Figure 6. Model for the first stage of bitumen formation through the asphaltene precipitation induced by the cooled magmatism-associated $CO_2$. Initially, it was the crude oil that was accumulated in the reservoir. Shortly after, the magmatism-derived $CO_2$ was charged into the reservoir from or accumulated at the top of the reservoir firstly and immediately induced the asphaltene precipitation at the contact (①). The continued charge of $CO_2$ resulted in a decreasing concentration gradient with depth within the reservoir inducing the precipitation of progressively less asphaltene from crude oil (②). A higher concentration of $CO_2$ induced the precipitation of more asphaltene in the higher position. Before the thermal cracking, the multiple $CO_2$ influxes may have driven the mobile fractions of crude oil away from the reservoir (③ ).

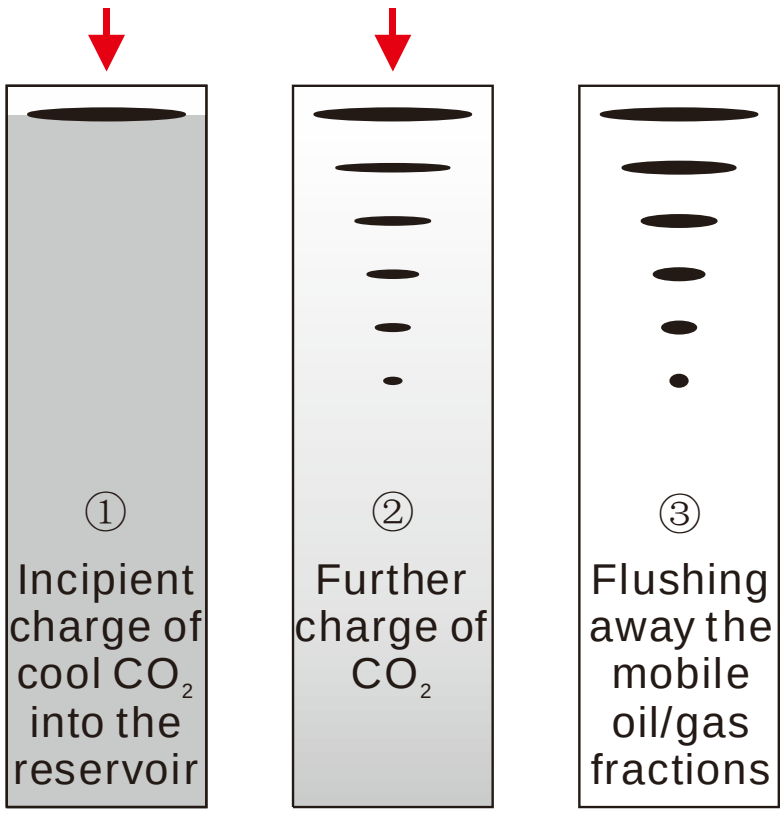

Figure 7. The Re and Os concentrations of the whole rock and bitumen versus depth. For the whole rock samples, the overall trend observed is the decrease in Re and Os concentrations with depth as shown in (a) and (b). For the bitumen, the Re concentrations increase with depth between 5300 and 5400 m (c), whereas the Os concentrations generally increase with depth (d).

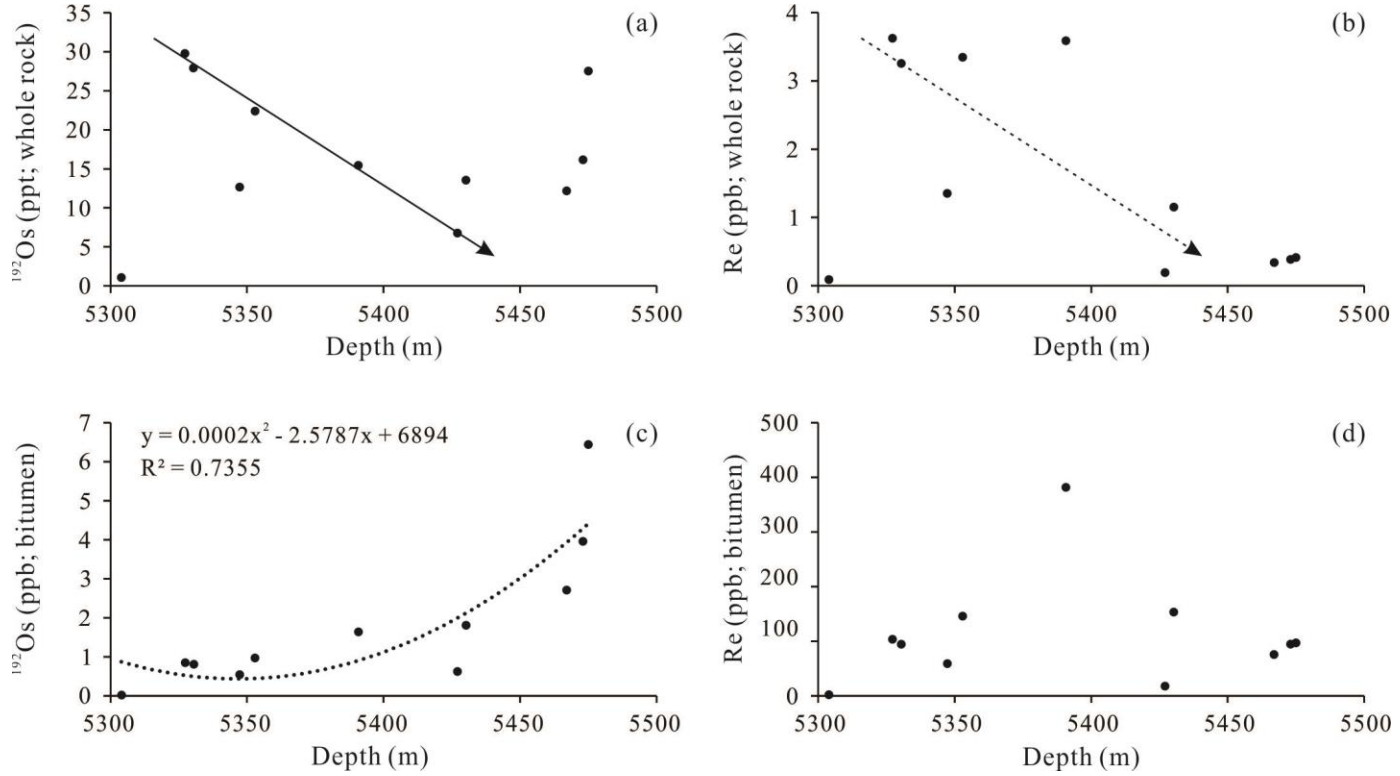

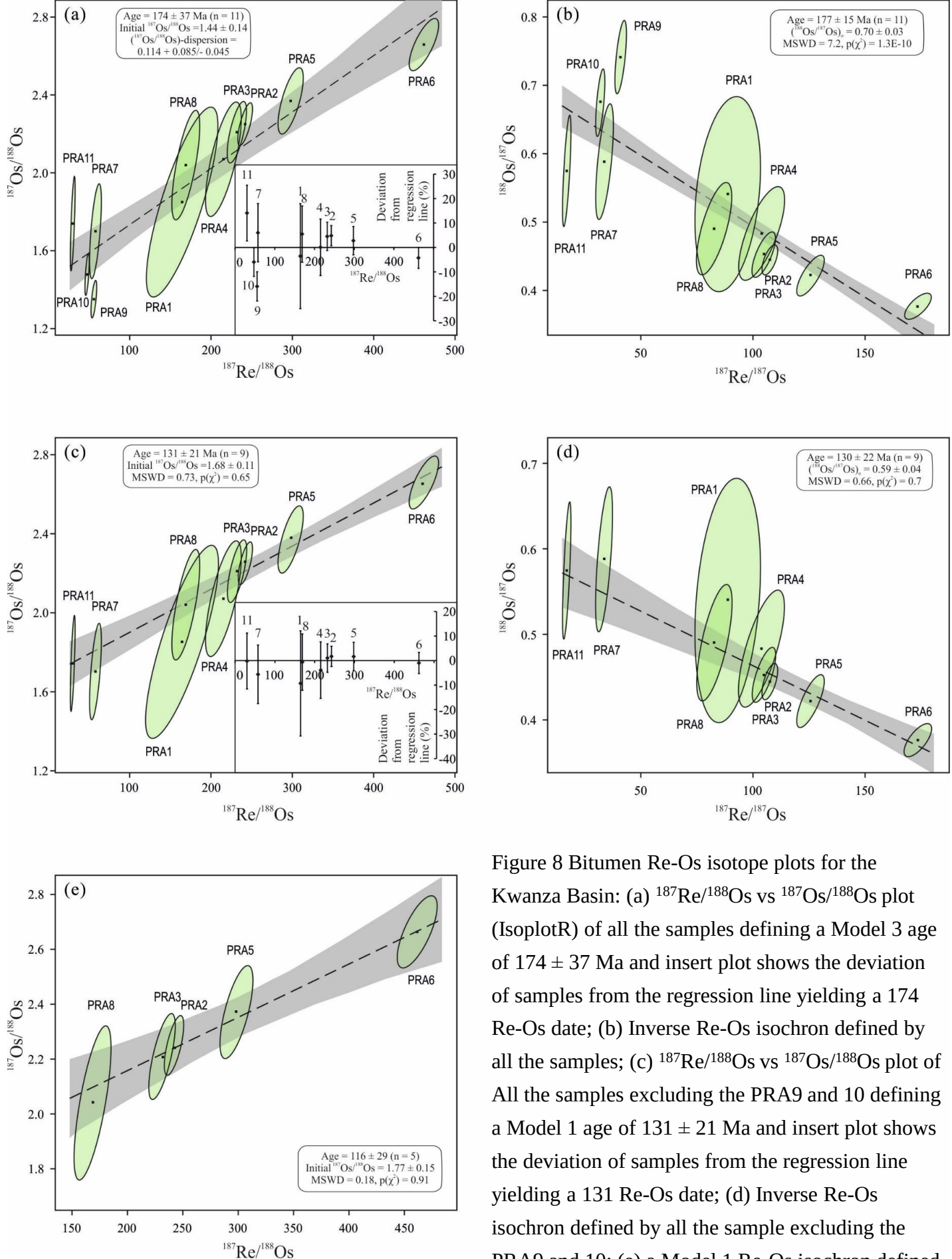


Figure 8 Bitumen Re-Os isotope plots for the Kwanza Basin: (a) $^{187}Re/^{188}Os$ vs $^{187}Os/^{188}Os$ plot (IsoplotR) of all the samples defining a Model 3 age of 174 ± 37 Ma and insert plot shows the deviation of samples from the regression line yielding a 174 Re-Os date; (b) Inverse Re-Os isochron defined by all the samples; (c) $^{187}Re/^{188}Os$ vs $^{187}Os/^{188}Os$ plot of All the samples excluding the PRA9 and 10 defining a Model 1 age of 131 ± 21 Ma and insert plot shows the deviation of samples from the regression line yielding a 131 Re-Os date; (d) Inverse Re-Os isochron defined by all the sample excluding the PRA9 and 10; (e) a Model 1 Re-Os isochron defined by the PRA2, 3, 5, 6, and 8 samples yielding an age of 116 ± 29 Ma which is the best estimate of the bitumen formation timing. See text for discussion.

Table 1 The TOC (bitumen) contents, Tmax and $BR_o$ of the Chela Formation samples

| Sample | Depth (m) | TOC | Tmax (°C) | $BR_o$ (%) |
|---|---|---|---|---|
| PRA1 | 5303.99 | 4.50% | 470 | / |
| TT1 | 5309.21 | 3.99% | 463 | 1.94 |
| PRA2 | 5327.26 | 3.50% | 456 | / |
| PRA3 | 5330.41 | 3.44% | 454 | / |
| PRA4 | 5347.31 | 2.33% | 445 | / |
| PRA5 | 5352.89 | 2.30% | 444 | / |
| TT2 | 5371.75 | 1.32% | 438 | 1.96 |
| PRA6 | 5390.73 | 0.94% | 437 | / |
| TT3 | 5408.69 | 0.99% | 435 | 1.88 |
| PRA7 | 5427.00 | 1.09% | 433 | / |
| PRA8 | 5430.19 | 0.75% | 430 | / |
| TT4 | 5450.00 | 0.71% | 431 | / |
| PRA9 | 5467.01 | 0.45% | 431 | / |
| PRA10 | 5472.99 | 0.41% | 428 | / |
| PRA11 | 5475.00 | 0.43% | 425 | / |
| TT5 | 5485.00 | 0.59% | 436 | / |
| TT6 | 5493.69 | 0.38% | 426 | 1.98 |

$BR_o$: Bitumen reflectance under white incident light in oil immersion.

Table 2 The composition and solubility of the Chela Formation bitumen.

| Sample | Mass (g) | Depth (m) | Pentane-extracts (oil and drilling mud) | DCM-extracts (asphaltene) | Rock-Eval TOC (insoluble bitumen) | Asphaltene/ (asphaltene + insoluble bitumen*) | Insoluble bitumen /(asphaltene + insoluble bitumen*) | ASCI of Asphaltene |
|---|---|---|---|---|---|---|---|---|
| 1 | 60 | 5300-5330 | 2.08% | 0.15% | 3.50% | 3% | 97% | 7 |
| | 90 | 5330-5350 | 3.67% | 0.10% | 2.30% | 3% | 97% | |
| 2 | 50 | 5370-5375 | 2.76% | 0.09% | 1.32% | 5% | 95% | 5 |
| | 50 | 5390-5395 | 1.65% | 0.07% | 0.94% | 6% | 94% | |
| | 50 | 5410-5415 | 3.06% | 0.11% | 1.09% | 8% | 92% | |
| 3 | 50 | 5430-5435 | 3.49% | 0.09% | 0.75% | 9% | 91% | Insufficient asphaltene |
| | 50 | 5450-5455 | 4.48% | 0.13% | 0.71% | 13% | 87% | |
| | 50 | 5470-5475 | 1.78% | 0.04% | 0.43% | 7% | 93% | |
| 4 | 500 | 5422-6015 | 2.39% | 0.05% | 0.54% | 8% | 92% | 1 |

* The insoluble bitumen contents here are converted from the TOC contents by dividing a coefficient of 0.83 arbitrarily.

Table 3 The Re-Os data synopsis of the Chela Formation samples and the $Os_i$ at the critical timings of the studied petroleum system.

| Sample | Depth (m) | Re (ppb) | ± | Os (ppt) | ± | $^{192}$Os (ppt) | ± | $^{187}$Re/$^{188}$Os | ± | $^{187}$Os/$^{188}$Os | ± | rho | $Os_i$ at 117 Ma | $Os_i$ at 131 Ma | $Os_i$ at 174 Ma |
|---|---|---|---|---|---|---|---|---|---|---|---|---|---|---|---|
| PRA1 | 5303.99 | 0.09(2.04) | 0.01 | 3.3(0.1) | 0.3 | 1.1(0.02) | 0.2 | 164 | 37 | 1.85 | 0.40 | 0.810 | 1.53 | 1.49 | 1.37 |
| PRA2 | 5327.26 | 3.63(103.66) | 0.01 | 92.1(2.6) | 1.7 | 29.8(0.85) | 0.9 | 242 | 7 | 2.25 | 0.09 | 0.712 | 1.77 | 1.72 | 1.54 |
| PRA3 | 5330.41 | 3.26(94.67) | 0.01 | 86.0(2.5) | 2.0 | 27.9(0.81) | 1.2 | 232 | 10 | 2.21 | 0.13 | 0.709 | 1.76 | 1.71 | 1.54 |
| PRA4 | 5347.31 | 1.37(58.91) | 0.01 | 38.5(1.7) | 1.5 | 12.7(0.54) | 1.1 | 215 | 18 | 2.07 | 0.24 | 0.714 | 1.65 | 1.60 | 1.44 |
| PRA5 | 5352.89 | 3.36(146.07) | 0.01 | 70.2(3.1) | 1.6 | 22.4(0.98) | 0.9 | 298 | 12 | 2.37 | 0.14 | 0.714 | 1.79 | 1.72 | 1.50 |
| PRA6 | 5390.73 | 3.59(381.82) | 0.01 | 49.8(5.3) | 1.0 | 15.5(1.64) | 0.5 | 462 | 15 | 2.66 | 0.11 | 0.736 | 1.76 | 1.66 | 1.32 |
| PRA7 | 5427.00 | 0.20(18.05) | 0.01 | 19.8(1.8) | 0.8 | 6.8(0.62) | 0.6 | 58 | 6 | 1.70 | 0.20 | 0.636 | 1.59 | 1.58 | 1.54 |
| PRA8 | 5430.19 | 1.15(153.80) | 0.01 | 41.1(5.5) | 1.6 | 13.6(1.81) | 1.1 | 169 | 14 | 2.04 | 0.23 | 0.713 | 1.71 | 1.67 | 1.55 |
| PRA9 | 5467.01 | 0.34(75.67) | 0.01 | 34.3(7.6) | 0.8 | 12.2(2.71) | 0.5 | 55 | 3 | 1.35 | 0.08 | 0.613 | 1.24 | 1.23 | 1.18 |
| PRA10 | 5472.99 | 0.39(94.58) | 0.01 | 46.4(11.3) | 1.0 | 16.3(3.97) | 0.7 | 47 | 2 | 1.48 | 0.09 | 0.623 | 1.39 | 1.38 | 1.35 |
| PRA11 | 5475.00 | 0.42(97.01) | 0.01 | 81.3(18.9) | 3.1 | 27.7(6.45) | 2.2 | 30 | 3 | 1.74 | 0.20 | 0.682 | 1.68 | 1.68 | 1.65 |

*The numbers in front of the brackets are the whole rock Re, Os and $^{192}$Os concentrations in ppb, ppt and ppt, respectively. The number in the brackets are the bitumen Re, Os and $^{192}$Os concentrations in ppb corrected from the whole rock concentrations by dividing the samples' TOC contents.

**The analytical results are all presented with 2 sigma errors.